MOLECULAR BIOLOGY

Nucleosomes represent a crucial target for the intra-S phase checkpoint in response to replication stress

Xiaoqin Liu[1,2]†, Bo Zhang[1]†, Yu Hua[1], Chuanqi Li[3]*, Xizhou Li[4]*, Daochun Kong[1]*

The intra-S phase checkpoint is essential for stability of stalled DNA replication forks. However, the mechanisms underlying checkpoint regulation remain poorly understood. This study identifies a critical checkpoint target—the ubiquitin E3 ligase Brl2, revealing a new dimension of checkpoint regulation. Upon replication fork stalling, Brl2 undergoes phosphorylation at five serine residues by Cds1^{Chk2} kinase, resulting in the loss of its ligase activity and a marked reduction in H2BK119ub1 levels. In the *brl2-5D* (the five serine residues are replaced with aspartic acid) and *htb-K119R* mutants, chromatin becomes highly compacted. Furthermore, the rates of stalled replication fork collapse, and dsDNA breaks are significantly reduced in *brl2-5D cds1^{Chk2}*Δ cells compared to *cds1^{Chk2}*Δ cells. Thus, this study demonstrates that nucleosomes are targeted by the intra-S phase checkpoint and highlights the checkpoint's critical role in configuring compact chromatin structures at replication fork stalling sites. These findings may explain why ATR and Chk1 are essential for cell proliferation and embryonic development, while ATM is not.

INTRODUCTION

Unlike prokaryotes, genomic DNA replication in eukaryotes occurs within the context of chromatin, which markedly complicates both the replication process and its regulation. The fundamental unit of chromatin is the nucleosome, comprising 147 bp of DNA that wrap nearly twice around an octamer core formed by two copies of each of the four types of histone proteins: H2A, H2B, H3, and H4 (*1*). Chromatin is generally classified into two structurally and functionally distinct forms—heterochromatin and euchromatin (*2*, *3*). Heterochromatin is characterized by high condensation and low gene density, while euchromatin is more relaxed and has relatively high gene density. Moreover, various chemical modifications, such as acetylation, ubiquitination, and methylation, can adjust the level of chromatin condensation, thereby influencing gene transcription, cell differentiation, and carcinogenesis (*3*–*6*).

During DNA replication, chromatin undergoes extensive transformation. Ahead of the replication fork, chromatin relaxes to facilitate the passage of the DNA replication fork through nucleosomes, resulting in nucleosome disassembly (*7*, *8*). Behind the replication fork, nucleosomes must be reassembled on the two daughter DNA strands to restore the chromatin structure. Whether it is the relaxation of chromatin ahead of the replication fork or the reassembly of chromatin behind it, several replication factors within the replisome complex—such as the minichromosome maintenance protein complex (MCM), proliferating cell nuclear antigen, and replication protein A (RPA)—play a direct role in these processes (*9*–*11*). Therefore, physical and biochemical interactions exist between the replisome and the nucleosomes surrounding the replication fork. This indicates that a eukaryotic replication fork comprises three major components: a replisome, a DNA fork, and the nucleosomes adjacent to the replisome (*12*).

Two major biochemical reactions occur at the replication fork: DNA unwinding catalyzed by the replicative helicase Cdc45-MCM-GINS (CMG) complex and the synthesis of leading and lagging strand DNA by DNA polymerases ε, δ, and α. These two biochemical reactions necessitate strict coordination. In eukaryotes, this coordination is achieved through Mrc1- and Ctf4-mediated interactions between the CMG helicase and DNA polymerases ε, δ, and α (*13*–*16*). However, because these protein interactions are not permanent, the Mrc1- and Ctf4-mediated interactions may occasionally break down. When this occurs, the CMG helicase can detach from the replication forks and move away, leading to replisome and replication fork collapse. Thus, because of the inherent fragility of protein-protein interactions, replisomes and replication forks are intrinsically unstable. During normal cell growth, replication fork arrest is primarily caused by the blockade of DNA polymerases (*12*). When a DNA polymerase is impeded, replisome collapse is substantially enhanced. The reason is that the CMG helicase, powered by adenosine triphosphate (ATP) hydrolysis, continues to advance, while the blocked DNA polymerases cannot follow and synthesize DNA, resulting in the physical separation of the helicase from the polymerases and subsequent fork collapse (*12*, *17*).

The number of natural replication barriers on eukaryotic chromatin is astonishing. A yeast genome has ~2×10^3 replicaiton barriers (*12*, *18*–*20*), while a human genome harbors ~6–8×10^5 intrinsic replication barriers (unpublished data). Most of these intrinsic replication barriers are secondary DNA structures that are transiently formed on lagging strand template during DNA replication, as every piece of lagging strand template has a chance to be in a state of single-strand DNA (ssDNA) with a length of ~150 to 200 nucleotides, since the synthesis of lagging chains lags slightly behind the synthesis of leading chains. If a ssDNA sequence can potentially form secondary structures, such as G4, triplexes, and hairpin structures, then it is very likely that a secondary structure will be formed. For example, human genomic DNA has ~7×10^5 sequences that can potentially form G4 structures (*19*). In addition, ~50% or more of human genomic DNA is either moderately or highly repetitive

[1]Peking-Tsinghua Center for Life Sciences, The National Laboratory of Protein and Plant Gene Research, College of Life Sciences, Peking University, Beijing 100871, China. [2]Institute of Brain Science, College of Medicine, Shanxi Datong University, Datong 037009, China. [3]Suzhou Institute for Advanced Research, University of Science and Technology of China, Suzhou 215123, China. [4]Department of Breast and Thyroid Surgery, Changhai Hospital, The Naval Military Medical University, Shanghai, China.
*Corresponding author. Email: dekeli@163.com (C.L.); lixizhou721@126.com (X.L.); kongdc@pku.edu.cn (D.K.)
†These authors contributed equally to this work.

sequences (*20*), and a high percentage of these repetitive sequencres can potentially form triplexes or other secodary structures (*21*, *22*). These secondary structures on lagging strand template will block DNA polymerase δ, resulting in replication fork stalling. Besides those secondary DNA structures, RNA-DNA hybrids, collision with transcription machinery, and some DNA-bound proteins also impede fork movement by either blocking replicative helicase or blocking DNA polymerases. Moreover, some DNA lesions on genome also block DNA replicaiton forks. Therefore, replication fork stalling is a highly frequent event. Replication fork stalling generates tremendous stress to DNA replication.

The intra-S phase checkpoint is crucial for maintaining the stability of stalled replication forks. In checkpoint-deficient cells, stalled replication forks collapse, leading to the formation of reversed replication forks (*23*, *24*), DNA breaks (*25*), dissociation of replisome factors from DNA (*26*, *27*), unscheduled DNA recombination (*28*, *29*), incomplete DNA replication (*30*), and premature mitotic entry (*31*–*33*). Conversely, in checkpoint-proficient cells, the stalling of replication forks activates the intra-S phase checkpoint, which then exerts regulatory effects on the stalled forks to enhance their stability (*12*, *34*–*36*). Current understanding of the underlying mechanisms of checkpoint regulation has advanced enormously, including the inhibition of late DNA replication origin firing through $Mec1^{ATR}$-$Rad53^{Chk2}$–mediated phosphorylation of the Sld3 protein and the Cdc7-Dbf4 kinase (*37*–*41*). In addition, regulation of Mus81, Exo1, Rad60, and SMARCAL1 plays a vital role in preventing damage to stalled forks (*42*–*45*). Recent studies have also identified Dna2 and the replicative helicase CMG complex as critical checkpoint targets for stabilizing stalled replication forks (*17*, *24*).

This study identifies the ubiquitin E3 ligase Brl2 as a critical target of the intra-S phase checkpoint. Upon stalling of DNA replication forks, Brl2 is phosphorylated at five serine residues—S192, S193, S194, S292, and S486—resulting in a loss of its ligase activity. Furthermore, this study demonstrates that when replication forks stall, the level of H2BK119 ubiquitination (H2BK119ub1) is markedly reduced, leading to substantial chromatin compaction. We elucidate the mechanistic relationship among replication fork stalling, Brl2 phosphorylation, loss of ligase activity, reduction of H2BK119ub1 levels, chromatin compaction, and the stability of stalled replication forks. Thus, nucleosomes surrounding stalled replication forks are targeted by the intra-S phase checkpoint, revealing a new aspect of checkpoint regulation. The findings also highlight the critical role of the intra-S phase checkpoint in the formation and maintenance of heterochromatin or compacted chromatin domains at sites of DNA replication fork stalling. Given the extensive influence of chromatin structures on various biological processes, the checkpoint's role in establishing compact chromatin structures may help clarify why ataxia telangiectasia and Rad3-related kinase (ATR) and checkpoint kinase 1 (Chk1) are essential for cell growth and embryonic development, while ataxia telangiectasia mutated (ATM) is not (*46*–*49*), despite its critical function in DNA damage response and maintenance of genomic integrity (*50*).

RESULTS

The *brl2*Δ mutant considerably suppresses the sensitivity of checkpoint-defective cells to hydroxyurea

To identify the targets of the intra-S checkpoint pathway in response to replication fork stalling, we selected $rad3^{ATR}\Delta$ mutant strains capable of growing on rich media containing 1 mM hydroxyurea (HU), as previously described (*17*). It is anticipated that some mutants able to grow on plates with 1 mM HU may harbor mutations in checkpoint targets. If these mutations mimic checkpoint regulation, then they would confer resistance to HU in checkpoint-defective $rad3^{ATR}\Delta$ cells. HU inhibits ribonucleotide reductase, leading to deoxynucleoside triphosphate depletion, which in turn causes replication fork stalling. $Rad3^{ATR}$ serves as the primary kinase in the intra-S checkpoint signaling pathway, making it essential for the stability of stalled replication forks (*12*, *23*–*25*, *28*, *30*).

Using the aforementioned method, we identified several dozen mutants within a $rad3^{ATR}\Delta$ background. These mutants were able to grow in plates containing 1 mM HU (fig. S1, A and B). Genomic DNA was extracted from these mutants and subjected to deep sequencing. The genes containing mutations were individually reintroduced into $rad3^{ATR}\Delta$ cells to determine which mutated gene confers HU resistance. Experiments revealed that the *brl2-Q236** mutation (indicated by *, a stop codon) markedly reduces the HU sensitivity of $rad3^{ATR}\Delta$ cells. Specifically, HU sensitivity was decreased by approximately 600-fold or more due to *brl2-Q236**, as assessed through a serial dilution assay on plates containing 1 mM HU (Fig. 1A, left). Given the extent of this reduction, Brl2 may be a critical target of the checkpoint pathway in response to replication fork stalling. Brl2 is a ubiquitin E3 ligase in fission yeast, consisting of 680 amino acids, with four coiled-coil domains and one RING-type zinc finger domain (Fig. 1A, right) (*51*). The RING-type zinc finger domain is essential for the interaction between E2 ubiquitin–conjugating enzymes and substrates (*52*). Therefore, the *brl2-Q236** mutation likely abolishes its E3 ligase activity, as the truncated *brl2-Q236** loses nearly two-thirds of its amino acid residues, including the essential RING-type zinc finger domain. Brl2 is highly conserved among eukaryotes, with homologs in humans and budding yeast identified as RNF20/RNF40 and Bre1, respectively (*53*, *54*). Brl2, together with another E3 ligase, namely Brl1, is responsible for monoubiquitination of H2BK119 in fission yeast (*55*). RNF20/RNF40 and Bre1 also ubiquitinate H2BK120 in humans and H2BK123 in budding yeast, respectively, which play crucial roles in modulating chromatin structure, regulating gene expression, and repairing double-strand DNA breaks (*56*–*58*).

The *brl2-Q236** mutation is likely a loss-of-function variant. To confirm this, we constructed a double mutant of *brl2*Δ and $rad3^{ATR}\Delta$. Serial dilution assays demonstrated that, similar to $rad3^{ATR}\Delta$ *brl2-Q236**, the HU sensitivity of the *brl2*Δ $rad3^{ATR}\Delta$ double mutant was markedly reduced. In contrast, the exogenous expression of wild-type (*wt*) Brl2 completely restored HU sensitivity in $rad3^{ATR}\Delta$ *brl2*Δ cells (Fig. 1B). Furthermore, the cell phenotype of $rad3^{ATR}\Delta$ cells was restored in $rad3^{ATR}\Delta$ *brl2*Δ + pBrl2 cells (Fig. 1C). These results indicate that the loss of Brl2 function substantially decreases the HU sensitivity of $rad3^{ATR}\Delta$ cells.

We also investigated the effects of *brl1*Δ, *brl2-*Δ*znf* (which deletes the C-terminal 627 to 680 amino acids, encompassing the RING-type zinc finger domain in Brl2) and *htb1-K119R* on the HU sensitivity of $rad3^{ATR}\Delta$ cells. As shown in Fig. 1D, the HU sensitivity of the $rad3^{ATR}\Delta$ mutant strain was substantially reduced in *brl1*Δ $rad3^{ATR}\Delta$, *brl2-*Δ*znf* $rad3^{ATR}\Delta$, and *htb1-K119R* $rad3^{ATR}\Delta$ cells, with the extent of reduction comparable to that observed in *brl2*Δ $rad3^{ATR}\Delta$. Similarly, the mutations *brl2*Δ, *brl1*Δ, *brl2-*Δ*znf*, and *htb1-K119R* also considerably suppressed the HU sensitivity of $cds1^{Chk2}\Delta$ cells (Fig. 1E). To assess whether *brl2*Δ and *htb1-K119R*

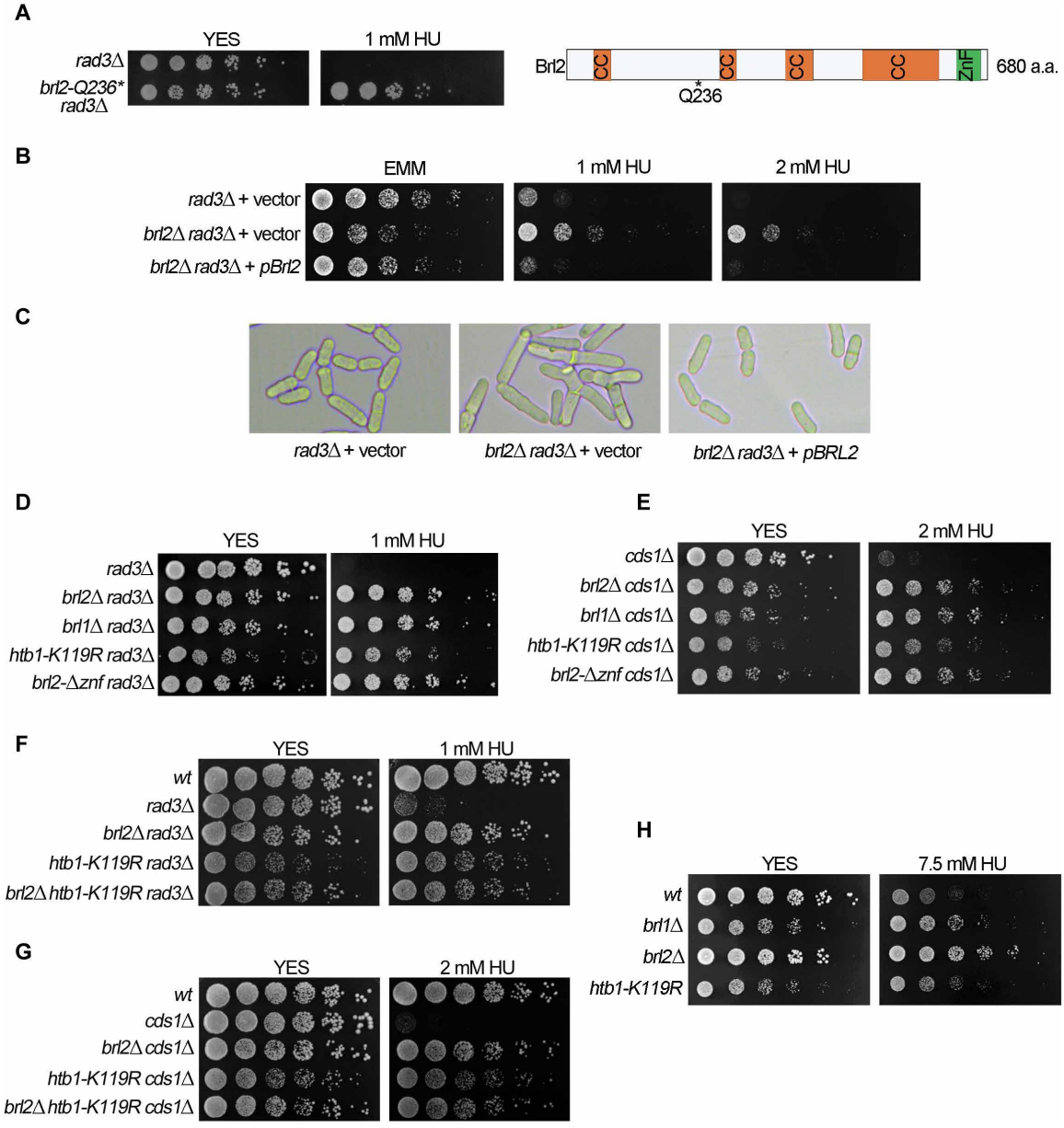

Fig. 1. Loss of Brl2 markedly suppresses the HU sensitivity of *wt*, *rad3^{ATR}*Δ, and *cds1^{Chk2}*Δ cells. (**A**) The *brl2-Q236** mutation markedly reduces the HU sensitivity of *rad3^{ATR}*Δ cells. Left: Fivefold serial dilution assay was performed to examine the HU sensitivity of *rad3^{ATR}*Δ cells and *brl2-Q236* rad3^{ATR}*Δ cells. Right: A schematic diagram showing the domain structure of Brl2. Location of mutant residue found in a screening experiment is indicated by an asterisk *, stop codon; CC, coiled-coil domain; ZnF, zinc finger domain; a.a., amino acid. (**B**) Fivefold serial dilution assay was performed to examine the HU sensitivity of *rad3^{ATR}*Δ, *brl2*Δ *rad3^{ATR}*Δ cells in the presence or absence of Brl2 expression. The indicated cells carrying a control empty plasmid (vector) or a plasmid expressing the *brl2* gene under the control of the *nmt1* promoter (*pBRL2*) were assayed on EMM containing different concentrations of HU. (**C**) Cell morphology. The indicated cells harboring a control empty plasmid or a plasmid expressing the *brl2* gene were grown in EHAL medium lacking thiamine for 16 hours at 30°C and directly imaged. (**D** to **H**) HU sensitivity of the *rad3*Δ, *brl2*Δ *rad3*Δ, *brl1*Δ *rad3*Δ, *htb1*-K119R *rad3*Δ, *brl2-*Δ*znf rad3*Δ, *cds1^{Chk2}*Δ, *brl2*Δ *cds1^{Chk2}*Δ, *brl1*Δ *cds1^{Chk2}*Δ, *htb1*-K119R *cds1^{Chk2}*Δ, *brl2-*Δ*znf cds1^{Chk2}*Δ, *brl1*Δ, *brl2*Δ, *htb1*-K119R, *brl2*Δ *htb1*-K119R *rad3*Δ, *brl2*Δ *htb1-K119R cds1^{Chk2}*, and *wt* cells. The strains were examined using a fivefold serial dilution assay, and plates were incubated at 30°C for 3 to 4 days. HU concentrations are indicated above each image.

exhibit an epistatic relationship in reducing the HU sensitivity of *rad3^{ATR}*Δ cells, we constructed a triple mutant of *brl2*Δ *rad3^{ATR}*Δ *htb1-K119R*. The results indicated that the double mutation of *brl2*Δ and *htb1-K119R* did not further decrease the HU sensitivity of either *brl2*Δ *rad3^{ATR}*Δ, *htb1-K119R rad3^{ATR}*Δ, *brl2*Δ *cds1^{Chk2}*Δ, or *htb1-K119R cds1^{Chk2}*Δ cells (Fig. 1, F and G). These findings suggest that (i) the reduction of H2BK119ub1 levels is critical for suppressing the HU sensitivity of *rad3^{ATR}*Δ and *cds1^{Chk2}*Δ cells; (ii) the deletion of Brl2 and H2B-K119 deubiquitination likely exhibits an epistatic relationship in response to replication fork stalling. Moreover, the HU sensitivity of *wt* cells is also noticeably reduced by *brl1*Δ, *brl2*Δ, and *htb1-K119R* mutations (Fig. 1H),

reinforcing the notion that Brl2 is a critical checkpoint target in response to replication fork stalling.

The level of H2BK119ub1 substantially decreases in response to replication fork stalling

We subsequently investigated the changes in H2BK119ub1 levels in response to replication fork stalling. Western blot analysis revealed the presence of two distinct H2B bands in the whole cell extracts from both *wt* and *htb1-3FLAG* cells (where H2B is tagged with three FLAG peptides at its C terminus). The molecular weights of these H2B bands are approximately 15 and 23 kDa in *wt* cells and approximately 20 and 28 kDa in *htb1-3FLAG* cells, respectively (Fig. 2A). The H2B subunit in the fission yeast *Schizosaccharomyces pombe* consists of 126 amino acids, with a calculated molecular weight of 13.819 kDa. Consequently, the faster-migrating band at approximately 15 kDa is likely the H2B subunit. In the *htb1-K119R-3FLAG* strain, the faster-migrating band remains detectable, whereas the slower-migrating band disappears (Fig. 2A), suggesting that the latter is likely derived from H2B ubiquitinated at K119. There is an approximate 8-kDa difference in molecular weight between the faster- and slower-migrating H2B bands (Fig. 2A). Given that a ubiquitin molecule has a molecular weight of approximately 8.6 kDa (*59*), it is plausible that the slower-migrating band corresponds to H2B monoubiquitinated at K119, as confirmed in Fig. 2B.

Furthermore, similar to *htb1-K119R* cells, the slower-migrating band was absent in *brl2*Δ cells (Fig. 2B, left), while the level of the slower-migrating band noticeably increased in *ubp8*Δ cells compared to *wt* cells (Fig. 2B, left). Ubp8, a deubiquitinase, specifically deubiquitinates H2BK119 in the fission yeast *S. pombe* (*60*, *61*). Moreover, Western blot analysis using a monoclonal antibody that specifically recognizes H2BK119ub1 confirmed that the slower-migrating band corresponds to H2B monoubiquitinated at K119 (Fig. 2B, right). On the basis of these findings, we conclude that (i) the slower-migrating band represents a monoubiquitinated H2B band; and (ii) the ubiquitin E3 ligase Brl2 is essential for the ubiquitination of H2B at K119, leading to the production of H2BK119ub1.

Considering that *brl2*Δ markedly reduces the sensitivity of *rad3*^{ATR}Δ or *cds1*^{Chk2}Δ to HU (Fig. 1, B to E), along with the necessity of Brl2 for the ubiquitination of H2BK119 (Fig. 2B), we investigated whether the level of H2BK119ub1 decreases in response to replication fork stalling. In an unsynchronized *wt* culture treated with HU for 1, 2, 3, or 4 hours, the levels of H2Bub1 gradually and apparently decreased (Fig. 2C). A statistical analysis of the H2Bub1/H2B ratio is also presented in Fig. 2C (right). During normal cell growth cycles in the fission yeast *S. pombe*, approximately 70% of cells are in the G_2 phase, while the remainder is equally distributed among G_1, S, and M phases. Consequently, a progressive reduction in H2Bub1 levels is observed in a synchronizing culture under HU treatment (Fig. 2C), as the deubiquitination of H2Bub1 occurs only when replication forks stall. We further examined whether the intra-S checkpoint is essential for the reduction of H2BK119ub1 levels by measuring H2BK119ub1 in *wt* and *cds1*^{Chk2}Δ cells with or without HU treatment. Both *wt* and *cds1*^{Chk2}Δ cells, under a *cdc25*^{ts} background, were arrested in the G_2/M phase at a restrictive temperature of 36.5°C for 3.5 hours and subsequently shifted to the permissive temperature of 26°C in the presence or absence of HU. Cell samples were collected at indicated time points, and the levels of H2B and H2BK119ub1 were assessed by Western blot analysis. As shown in Fig. 2D (left) (mock treated), the levels of H2B and H2BK119ub1 in both *wt* and *cds1*^{Chk2}Δ cells remained largely constant from 60 to 120 min without HU treatment following G_2/M release. However, in the presence of HU, H2BK119ub1 levels decreased markedly in *wt* cells (Fig. 2D, right), whereas levels remained unchanged in *cds1*^{Chk2}Δ cells even with HU treatment (Fig. 2D, right). A statistical analysis of the H2Bub1/H2B ratio is also included in Fig. 2D. Thus, on the basis of the results shown in Fig. 2 (C and D), we conclude that (i) H2BK119ub1 is deubiquitinated in response to replication fork stalling, and (ii) the intra-S checkpoint kinase Cds1^{Chk2} is necessary for the reduction of H2BK119ub1 levels.

Brl2 is phosphorylated in response to replication fork stalling

The results presented in Figs. 1 and 2 indicate that Brl2 may be a target of the intra-S checkpoint in response to replication fork stalling. Therefore, we investigated whether Brl2 is phosphorylated under conditions of replication fork stalling. As shown in the left of Fig. 3A, slowly migrating bands of Brl2 were detected in Phos-tag gel in the presence of HU but not in its absence. In addition, these slowly migrating Brl2 bands were absent in checkpoint-defective *rad3*^{ATR}Δ or *cds1*^{Chk2}Δ cells, even when HU was present (Fig. 3A, right). To determine whether Cds1^{Chk2} could directly phosphorylate Brl2, we purified Brl2 and activated Cds1^{Chk2} as described in Materials and Methods (Fig. 3B, left and middle). The results in the right of Fig. 3B show the presence of slowly migrating bands when Cds1^{Chk2} was included, indicating that Cds1^{Chk2} can directly phosphorylate Brl2 in vitro. Collectively, these findings suggest that Brl2 is phosphorylated during replication fork stalling, with Cds1^{Chk2} being responsible for the phosphorylation of Brl2 detected in vivo.

Cds1^{Chk2} phosphorylates Brl2 at five specific serine residues of S192, S193, S194, S292, and S486

A survey of the amino acid sequence of Brl2 identified 6 SQ/TQ motifs for Rad3^{ATR} and 19 RxxS/T motifs for Cds1^{Chk2} (Fig. 4A) (*62*–*64*). The locations of these potential Rad3^{ATR} and Cds1^{Chk2} phosphorylation sites in Brl2 are illustrated in Fig. 4A (left). Preliminary testing was conducted to determine whether phosphorylation of these sites results in a physiological phenotype. Consequently, all sites were mutated to either alanine (phospho-deficient) or aspartic acid (potential phospho-mimic), yielding the constructs *brl2-6A/D* (where the 6 Rad3^{ATR}-recognized serine and threonine residues are mutated to alanine or aspartic acid, respectively) and *brl2-19A/D* (where the 19 Cds1^{Chk2}-recognized serine and threonine residues are similarly mutated). These *brl2-6A/D* and *brl2-19A/D* mutant genes were introduced into *rad3*^{ATR}Δ and *cds1*^{Chk2}Δ cells to replace the original *brl2* gene. Results indicated that *brl2-6A*, *brl2-6D*, and *brl2-19A* cells exhibited comparable growth on yeast extract sucrose (YES) plates, although *brl2-19D* displayed slightly reduced growth (Fig. 4A, right). Furthermore, the phospho-mimic mutation at the six ATR recognition sites (*brl2-6D*) did not confer resistance to HU in *rad3*^{ATR}Δ cells (Fig. 4A, right). In contrast, *brl2-6A rad3*^{ATR}Δ and *brl2-6D rad3*^{ATR}Δ cells were more sensitive to HU than *rad3*^{ATR}Δ cells (Fig. 4A, right). These results suggest that ATR likely neither phosphorylates Brl2 nor regulates its function in response to replication fork stalling. However, similar to *brl2-Q236** and *brl2*Δ, the phospho-mimic mutation *brl2-19D*

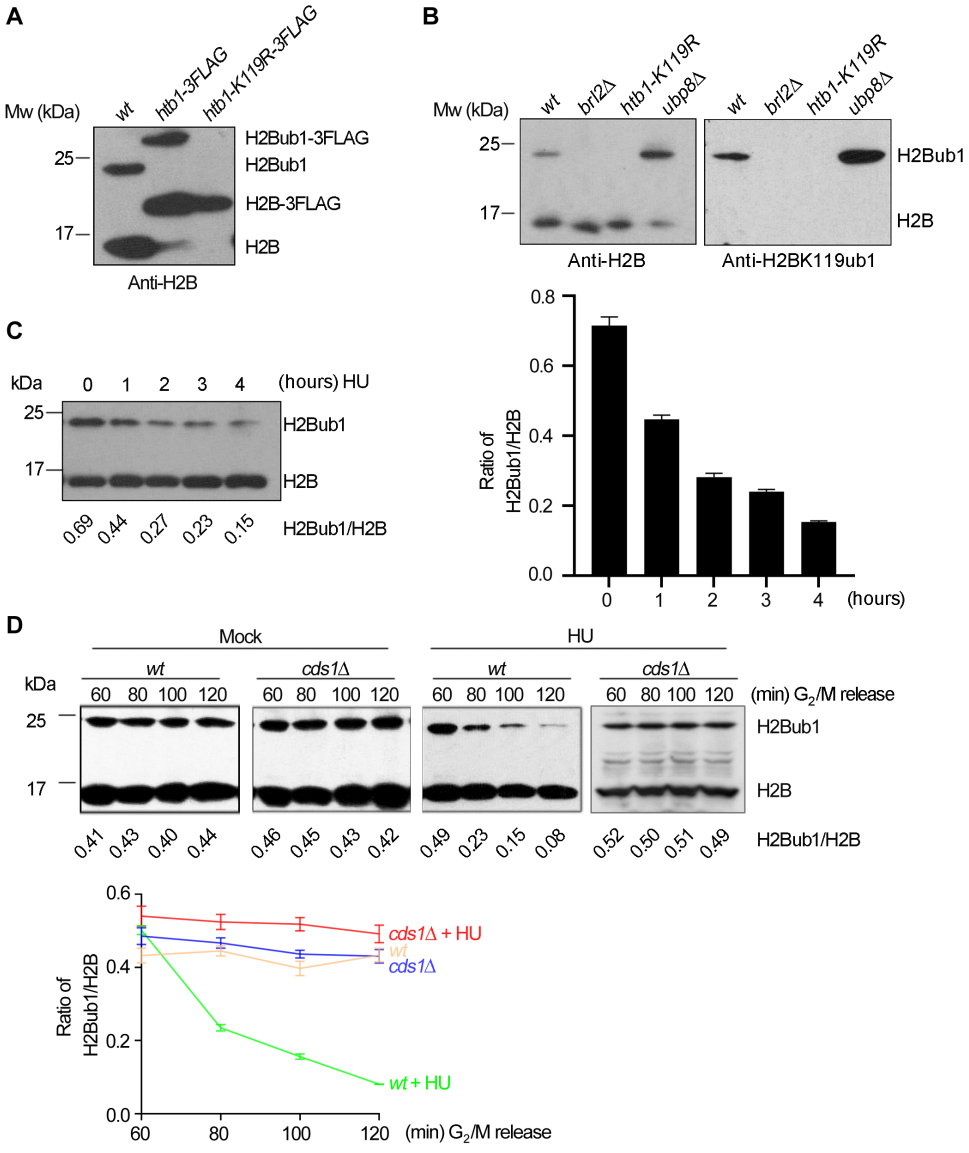

Fig. 2. The level of H2BK119ub1 is remarkably down-regulated by HU treatment. (**A** and **B**) The antibody against H2B is effective to probe the H2B protein and its ubiquitination on K119. (A) Anti-H2B Western blots on the whole cell extracts (WCEs) prepared from an untagged strain (*wt*) and the tagged strains (*htb1-3FLAG* and *htb1-K119R-3FLAG*). (B) WCEs from *wt*, *brl2*Δ, *htb1-K119R*, and *ubp8*Δ were probed with anti-H2B and anti-H2BK119ub1. Bands corresponding to H2B and H2Bub1 are indicated on the right, and the molecular marker is shown on the left. (**C**) Western blot quantification of the ratio of ubiquitinated H2B to H2B level after HU treatment. Left: *wt* cells were treated with 12.5 mM HU or not, and aliquots were taken at the indicated times. WCEs were prepared and probed with anti-H2B. The band intensity was quantified by the imageJ software (National Institutes of Health, Bethesda, MD, USA). The ratio of the H2Bub1 level to H2B level at each time point was calculated. Right: A statistical analysis of the ratio of the H2Bub1 level to H2B level at each time point after HU treatment. (**D**) WCEs with HU treatment or not were analyzed by Western blot analysis using antibody against H2B. Top: *wt* (*cdc25-22*) and *cds1*^{Chk2}Δ *cdc25-22* cells were blocked for 3 hours at 36.5°C and then shifted to 26°C in the presence or absence of 12.5 mM HU. Cells were harvested at the indicated time after G_2/M release. Bottom: A statistical analysis of the ratio of H2Bub1/H2B versus the time of HU treatment after G_2/M release. Mw, molecular weight.

markedly reduced HU sensitivity in *cds1*^{Chk2}Δ cells (Fig. 4A, right). Together with the findings in Fig. 3B, these results suggest that the function of Brl2 is likely regulated by Cds1^{Chk2} in response to replication fork stalling.

To identify phosphorylation sites on Brl2, we isolated Brl2 from HU-treated *wt* cells and subsequently conducted mass spectrometry (MS) analysis. In addition, MS analysis was performed on Brl2 that had been phosphorylated in vitro by purified Cds1^{Chk2}. Both MS analyses revealed that Brl2 was phosphorylated at S192, S193, S194, S292, and S486 (Fig. 4B and fig. S2, A to E). Among these five serine phosphorylation sites, S194 and S292 are situated within the consensus Cds1^{Chk2} phosphorylation motif (Fig. 4C). Notably, S194, S292, and S486 are conserved between the fission yeast *S. pombe* and the budding yeast *Saccharomyces cerevisiae*, whereas S192 is mutated to aspartic acid and S193 to glutamic acid, both of which represent a phospho-mimic state (Fig. 4C). These findings

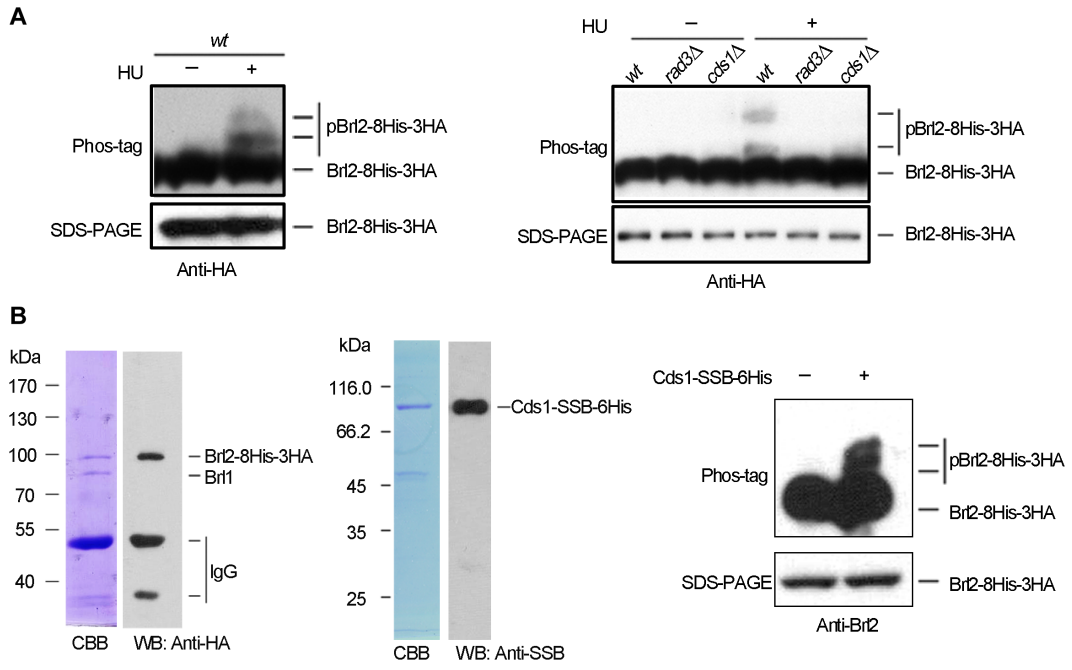

Fig. 3. Cds1^{Chk2} regulates Brl2 phosphorylation in vivo and in vitro. (**A**) The WCEs from *wt*, *rad3^{ATR}*Δ, and *cds1^{Chk2}*Δ cells with or without HU treatment were separated by 25 μM Phos-tag SDS-PAGE to detect the phosphorylated shift with anti-HA (Brl2 is tagged with 8His and 3HA). (**B**) Cds1^{Chk2} phosphorylates Brl2 in vitro. Left and middle: Brl2-8His-3HA and Cds1-SSB-6His were purified to homogeneity. The *brl2-8his-3HA* was integrated into the *S. pombe brl2* locus to express Brl2-8His-3HA under the control of the native *brl2* promoter. Brl2-8His-3HA was purified to apparent homogeneity by Ni-NTA chromatography and using HA beads. Cds1-SSB-6His was overexpressed under the *nmt1* promoter in *S. pombe* cells with HU treatment to ensure its activity and purified by ammonium sulfate precipitation and Ni-NTA chromatography. Right: Cds1-catalyzed phosphorylation of Brl2 was performed at 37°C for 25 min with or without kinase Cds1-SSB-6His. The products were detected by 25 μM Phos-tag SDS-PAGE and immunoblotted using anti-Brl2. IgG, immunoglobulin G. CBB, Coomassie Brilliant Blue; WB, Western blot.

indicate that the kinase Cds1^{Chk2} can phosphorylate these serine sites both in vivo and in vitro. To verify phosphorylation of these sites in cells, we generated three phosphorylation-specific antibodies targeting phosphorylated S192/193/194, S292, and S486 (pS192/193/194, pS292, and pS486) separately. Dot blot analysis confirmed that these antibodies specifically recognize the phosphorylated peptides while not detecting nonphosphorylated peptides (fig. S2F). In *wt* cells, signals for pS192/193/194, pS292, and pS486 were observed in samples collected after 1 hour of HU treatment (Fig. 4D, left) and increased in a time-dependent manner, whereas these signals were faint in mock-treated cells (Fig. 4D, right). Furthermore, the signals for pS192/193/194, pS292, and pS486 completely disappeared from HU-treated *cds1^{Chk2}*Δ and *brl2-5A* cells (where all five serine residues are mutated to alanine) (Fig. 4D, left), suggesting that Cds1^{Chk2} is the primary kinase responsible for phosphorylating Brl2 at these sites. In addition, Phos-tag gel band mobility shift assays indicated that only the S192, S193, S194, S292, and S486 residues were phosphorylated, as slowly migrating bands were absent in *brl2-5A* cells under HU treatment (Fig. 4E). Collectively, these results lead us to conclude that S192, S193, S194, S292, and S486 of Brl2 are direct targets of Cds1^{Chk2}. Moreover, the activation of Cds1^{Chk2} was unaffected in *brl2-5A* and *brl2-5D* cells (where S192, S193, S194, S292, and S486 are mutated to aspartic acid), as the phosphorylation levels of Cds1^{Chk2} were similar among *wt*, *brl2-5A*, and *brl2-5D* cells (Fig. 4F). This finding suggests that checkpoint activation in response to replication fork stalling is not altered in *brl2-5A* and *brl2-5D* cells.

Cds1^{Chk2}-mediated phosphorylation of Brl2 markedly reduces H2BK119ub1 levels and promotes chromatin condensation

To evaluate the importance of Cds1^{Chk2}-mediated phosphorylation of Brl2 in response to replication fork stalling, the five serine residues (S192-S193-S194, S292, and S486) were all mutated together to either alanine (*brl2-5A*, phosphor deficient) or aspartic acid (*brl2-5D*, potential phosphor mimic). The mutated genes were individually introduced into *wt*, *cds1^{Chk2}*Δ, or *rad3^{ATR}*Δ strain. Serial dilution assays show that the *brl2-5D* mutation substantially reduced the HU sensitivity of *cds1^{Chk2}*Δ cells by about 125- to 625-fold, based on the serial dilution assay on plates containing 2 mM HU (Fig. 5A). The *brl2-5D* mutation also substantially reduced the sensitivity of *rad3^{ATR}*Δ cells by ~125- to 625-fold (Fig. 5B). Moreover, the *brl2-5D* mutation even increased the resistance of *wt* cells to HU by ~5- to 25-fold (Fig. 5C). Conversely, the *brl2-5A* mutation exhibited slightly greater sensitivity to HU compared to *wt* cells (Fig. 5C and fig. S3). These results indicate that Brl2 is a critical checkpoint target for the stability of stalled replication forks. As anticipated, *brl2-5A* mutation did not confer *cds1^{Chk2}*Δ, *rad3^{ATR}*Δ, and *wt* cell resistance to HU (Fig. 5, A to C).

To explore the mechanism of why *brl2-5D* confers the checkpoint-deficient cell resistance to HU, the cellular level of Brl2-5D was first examined. The result shown in Fig. 5D indicates that, compared to Brl2 in *wt* cells, the cellular levels of Brl2-5D or Brl2-5A did not decrease. The yeast two-hybrid assays indicate that the interaction between Brl1 and Brl2-5D or Brl2-5A was not altered either, compared to the interaction of Brl1 and Brl2 (Fig. 5E). However,

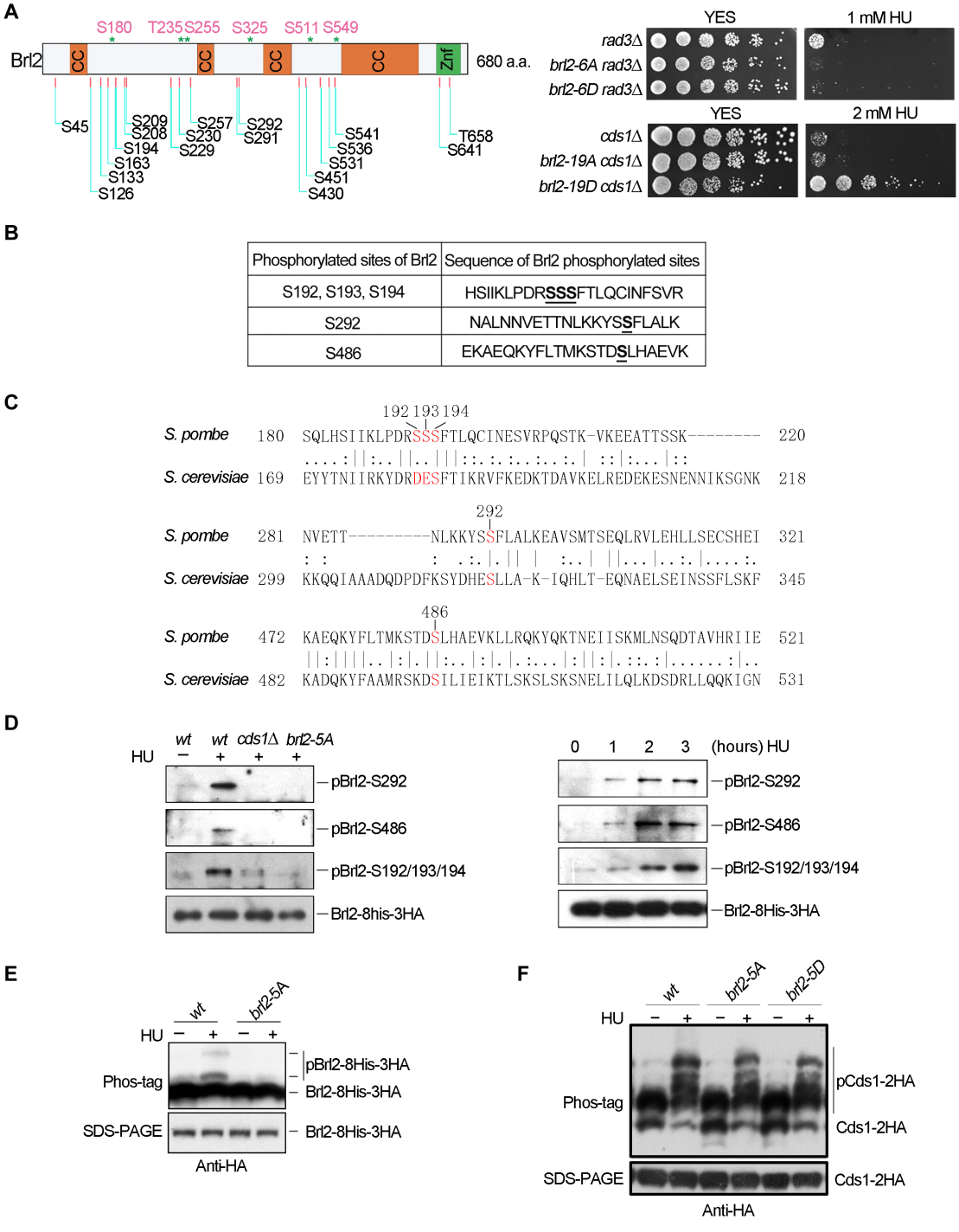

Fig. 4. Cds1^{Chk2} phosphorylates Brl2 on five serine residues in response to replication fork stalling. (**A**) Left: Distribution of 6 Rad3 targeted SQ/TQ motifs (top) and 19 Cds1 targeted RxxS/T cluster domains (bottom). Right: HU sensitivity of the indicated strains was examined by fivefold serial dilution assays in the presence or absence of HU. The 6 Rad3^{ATR}-targeted or 19 Cds1^{Chk2}-targeted serine and threonine residues were all mutated to either alanine (*brl2-6A* or *brl2-19A*) or aspartic acid (*brl2-6D* or *brl2-19D*). Cells in the log phase were serially diluted, plated on YES plates containing 1 mM HU or no HU, incubated at 30°C for 4 days, and imaged. (**B**) Cds1^{Chk2} phosphorylates Brl2 on S192, S193, S194, S292, and S486 in response to replication fork stalling. Brl2 was isolated from HU-treated cells and subjected to MS analysis. MS analysis was also performed with Brl2 phosphorylated by Cds1^{Chk2} in vitro. (**C**) The amino acid sequences around the five Cds1^{Chk2}-phosphorylated serine residues are shown. (**D**) Phosphorylation of Brl2 on S192, S193, S194, S292, and S486 in response to replication fork stalling induced by HU. Left: Western blot analysis of Brl2 phosphorylation at S192, S193, S194, S292, and S486 sites in *wt*, *cds1*^{Chk2}Δ, and *brl2-5A* (the five serine residues were all mutated to alanine) cells with HU treatment. Right: Western blot analysis of Brl2 phosphorylation at 192, 193, 194, 292, and 486 sites at different time points in HU-treated *wt* cells. (**E**) WCEs from *wt* and *brl2-5A* with HU treatment or not were separated by 25 μM Phos-tag SDS-PAGE (top) and SDS-PAGE (bottom) and then probed with anti-HA. (**F**) Cds1-2HA was isolated from *wt*, *brl2-5A*, and *brl2-5D* (the five serine residues were all mutated to aspartic acid) and separated by 25 μM Phos-tag SDS-PAGE (top) and SDS-PAGE (bottom), followed by immunoblotting analysis with the antibody against HA.

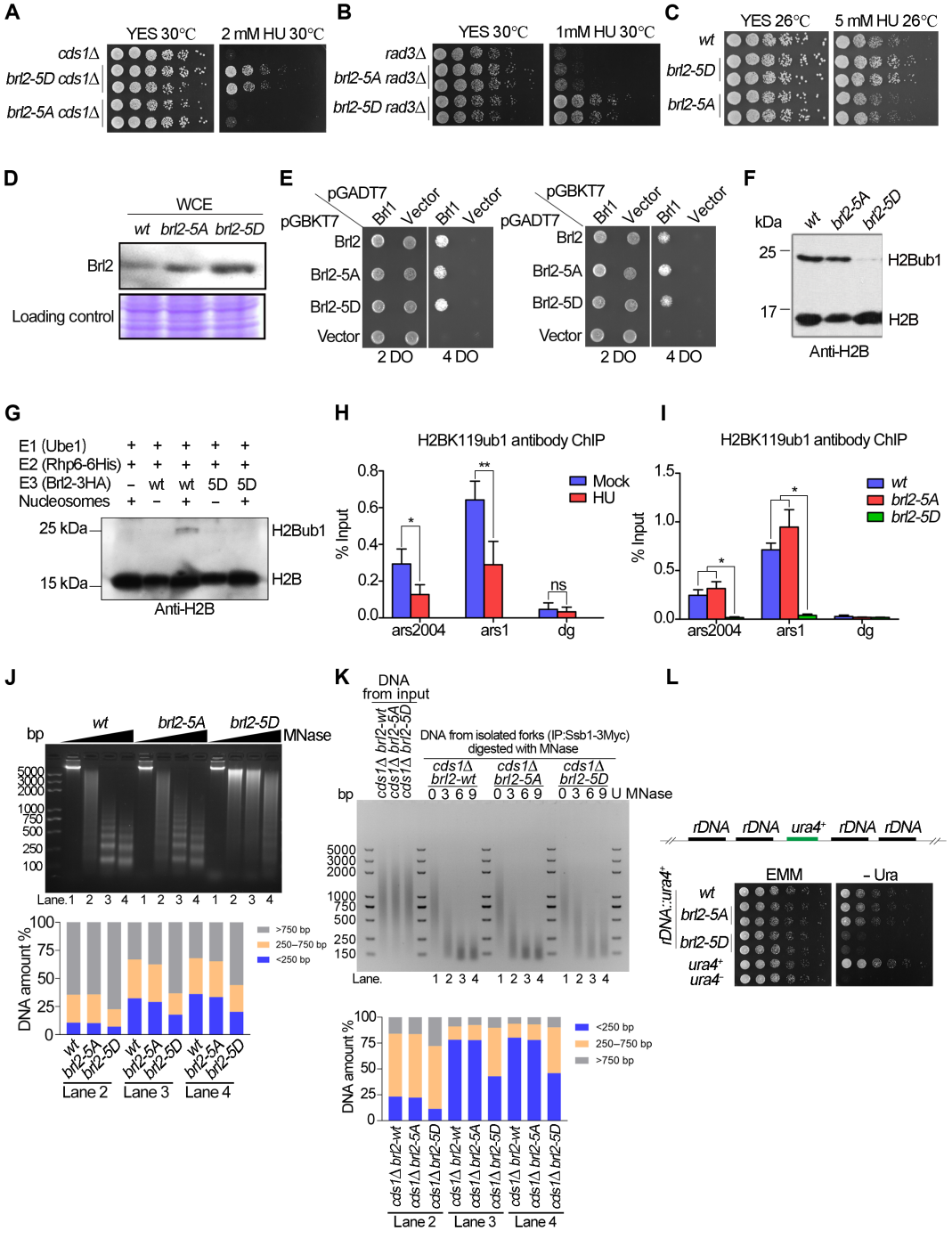

Fig. 5. Cds1^{Chk2}-mediated Brl2 phosphorylation leads to decreased H2BK119ub1 levels and chromatin condensation. (**A** to **C**) The HU sensitivity of indicated cells was measured by fivefold serial dilution assays with indicated HU concentrations and growth temperatures. (**D**) Western blot analysis of WCEs from *wt*, *brl2-5A*, and *brl2-5D* with anti-Brl2. (**E**) Yeast two-hybrid assays of measuring the interaction between Brl1 and Brl2-5A or Brl2-5D. These assays were performed on dropout (DO) plates: 4DO (SD-adenine, -histidine, -leucine, and -tryptophan) and 2DO (SD-leucine and -tryptophan). (**F**) Western blot analysis of WCEs from *wt*, *brl2-5A*, and *brl2-5D* cells with anti-H2B. (**G**) The in vitro assay of H2B E3 ligase activity of Brl2 and Brl2-5D. (**H**) ChIP-qPCR analysis of H2BK119ub at *ars2004* and *ars1* origins in *wt* cells treated with or without HU. The *wt* (*cdc25-22*) cells were blocked for 3 hours at 36.5°C and then shifted to 26°C in the presence or absence of 12.5 mM HU. Cells were harvested at 80 min after G_2/M release without HU treatment and 2.5 hours with HU treatment and then analyzed by ChIP-qPCR analysis. (**I**) ChIP-qPCR analysis of H2BK119ub1 around stalling replication forks at *ars2004* and *ars1* in *wt*, *brl2-5A*, and *brl2-5D* cells treated with HU. The cells in semi-log phase were treated with 12.5 mM HU at 30°C for 3 hours and then harvested for ChIP-qPCR analysis. The *dg* locus at centromere region was used as a negative control for H2BK119ub1. The *y* axis shows the percentage of input recovery. Results are expressed as the mean ± SD. (**J**) MNase digestion of chromatin from *wt*, *brl2-5A*, and *brl2-5D* cells. (**K**) MNase digestion of stalled replication forks together with neighboring chromatin that were isolated from the indicated cells. [(J) and (K), bottom] Analysis of relative percentage of different size of DNA fragments. (**L**) *brl2-5D* enhances the silencing of *rDNA::ura4*$^+$ reporter. Fivefold serial dilutions of indicated cells were plated on medium without uracil to monitor *rDNA::ura4*$^+$ expression.

compared with *wt* cells, the level of H2BK119ub1 was markedly reduced in *brl2-5D* cells, while the level of H2BK119ub1 was almost equal in *brl2-5A* or *wt* cells (Fig. 5F). This result explains why *brl2-5D* confers the $cds1^{Chk2}\Delta$, $rad3^{ATR}\Delta$ cell resistance to HU (Fig. 5, A and B), as deubiquitination of H2BK119 reduces HU sensitivity of checkpoint-deficient cells (Fig. 1, D and E).

The in vitro analysis system confirmed that Brl2-5D markedly reduced its ubiquitin E3 ligase activity, as the reaction product of H2Bub1 was easily detected with Brl2 but not with Brl2-5D (Fig. 5G). This result is consistent with a marked reduction of H2Bub1 level in the *brl2-5D* cells (Fig. 5F). The results presented in Fig. 5F, together with the results shown in Fig. 2 (C and D), suggest that a decreased H2BK119ub1 level confers cell resistance to HU-induced replication stress. Thus, we further performed chromatin immunoprecipitation and quantitative polymerase chain reaction (ChIP-qPCR) to determine the H2BK119ub1 levels around stalling replication forks at *ars2004* and *ars1* replication origins using antibodies against H2BK119ub1. Centromeric *dg* repeats, which are assembled into heterochromatin and have relatively low levels of H2BK119ub1 (*55*), were also measured as a negative control. We found that H2BK119ub1 is significantly reduced around stalling forks at *ars2004* and *ars1* origins in *wt* cells in response to HU treatment (Fig. 5H). However, a slight increase of H2BK119ub1 level was detected in *brl2-5A* cells compared with that in *wt* cells after HU treatment (Fig. 5I). In HU-treated *brl2-5D* cells, the level of H2BK119ub1 decreased sharply and was barely detectable (Fig. 5I). Together, these results indicate that the decrease of the H2BK119ub1 level is regulated by Brl2 phosphorylation in the presence of HU not only in the global chromatin but also in the nucleosomes at stalled replication forks.

A reduced H2Bub1 level is required for heterochromatin initiation and maintenance (*65*–*67*). This suggests that H2Bub1 plays a critical role in establishing basic structures of euchromatin and heterochromatin. Brl2 is required for H2BK119ub1. Thus, we examined the effect of *brl2-5D* mutation on global chromatin structure. Using micrococcal nuclease (MNase) digestion (*68*), we observed that the digestion pattern of *brl2-5A* was comparable to that of *wt* cells, while chromatin from *brl2-5D* exhibited notable resistance to MNase digestion (Fig. 5J, top). A quantitative analysis of chromatin resistance to MNase digestion is also presented (Fig. 5J, bottom).

To further investigate the compaction of chromatin at the stalling fork sites in the *brl2-5D* background, we conducted an additional experiment. Cells with the *cds1*Δ *brl2-wt*, *cds1*Δ *brl2-5A*, and *cds1*Δ *brl2-5D* genotypes were treated with HU for 4 hours to arrest replication forks. Subsequently, formaldehyde was added to the cultures for cross-linking replisome–DNA replication sites. Chromatin was then isolated from these cells and sonicated to achieve average fragment sizes ranging from 500 to 3000 bp (Fig. 5K). Replication forks were isolated using immunoprecipitation against Myc [*Ssb1*-3Myc, where the large subunit (Ssb1) of RPA is tagged with 3Myc], followed by MNase digestion. The results presented in Fig. 5K demonstrate that chromatin at the stalled replication fork sites in *cds1*Δ *brl2-5D* cells is substantially more compacted compared to the other two strains, which exhibited similar levels of chromatin compaction. In this assay, all three strains with the *cds1*Δ background were used to specifically evaluate the effect of the *brl2-5D* mutation on chromatin compaction at replication fork stalling sites.

These results indicate that *brl2-5D* reduces the level of H2BK119ub1 and promotes global chromatin compaction (Fig. 5, F, G, and I to K). Chromatin compaction in *brl2-5D* cells was further evaluated by analyzing gene expression. The $ura4^{+}$ reporter gene was inserted into the ribosomal DNA (rDNA) region to evaluate the local chromatin structure by monitoring rDNA::*ura4* expression. The strain carrying a normal copy of *ura4* was the positive control and that carrying the $ura4^{-}$ (deletion) gene was the negative control. The *wt* and *brl2-5A* cells showed a similar growth phenotype on medium lacking uracil, while the *brl2-5D* mutation impaired the ability of rDNA::*ura4* cells to form colonies on uracil-free plates (Fig. 5L). This result indicates that cells with the *brl2-5D* mutation exhibit enhanced silencing of the rDNA::*ura4* region, again suggesting that the chromatin in *brl2-5D* cells is more compact at the rDNA region than that in *wt* and *brl2-5A* cells. Together, the above findings demonstrate that Cds1 phosphorylates Brl2 at five serine positions, thereby reducing the H2BK119ub1 level, which ultimately leads to chromatin compaction at stalled replication forks.

brl2-5D prevents stalling replication forks from collapsing

Replication fork speed can indirectly reflect chromatin structure and stability of replication forks in a cell line. Thus, the speed of replication forks was examined in various cell lines in the absence of HU. As shown in Fig. 6A, the fork speed in *brl2-5D* background was significantly slower compared to that in *wt* or *brl2-5A* cells no matter that it was in the checkpoint-proficient or checkpoint-deficient cells. In addition, we examined the rate of DNA origin firing in the *brl2* mutant cells, and it was found that the rate of DNA replication origin firing is not affected in the *brl2-5A*, *brl2-5D*, and *brl2*Δ cells compared to *wt* cells (fig. S4). Next, we measured the fork speed in the presence of HU and after release from HU arrest. As shown in Fig. 6B, the fork speed was relatively similar in *wt* and *brl2-5A* cells but was significantly slower than that in *brl2-5D* cells. These results again suggest that the chromatin structure in *brl2-5D* cells is more compact compared to that in *wt* and *brl2-5A* cells, which is consistent with the results shown in Fig. 5 (J to L). The fork speed in a $cds1^{Chk2}\Delta$ background was relatively faster than that in *wt* cells in the presence of HU (Fig. 6B), consistent with a previous study (*17*). Similarly, the fork speed in *brl2-5D* $cds1^{Chk2}\Delta$ was significantly slower than that in $cds1^{Chk2}\Delta$ and *brl2-5A* $cds1^{Chk2}\Delta$ cells (Fig. 6B), reinforcing that *brl2-5D* cells have more compact chromatin. The speed of replication forks was also examined in these cell lines following the release from HU arrest. As shown in Fig. 6C, the fork recovery in *brl2-5D* was significantly better than that in *wt* and *brl2-5A* cells, leading to longer DNA fibers. The efficiency of fork recovery was in the following order: *brl2-5D* > *wt* ≥ *brl2-5A* cells (Fig. 6C), which is consistent with their resistance to HU (Fig. 5, A to C). The fork recovery was worse in a $cds1^{Chk2}\Delta$ background compared to *wt* cells; however, *brl2-5D* significantly increased the recovery rate of the $cds1^{Chk2}\Delta$ cells (Fig. 6C). Again, the rate of fork recovery is consistent with their resistance to HU (Figs. 5, A to C, and 6C).

To assess whether the stability of replication forks is enhanced by $Cds1^{Chk2}$-mediated phosphorylation of Brl2, we analyzed DNA fibers to determine the frequency of collapsed stalled forks under HU stress across different cell lines. Cells treated with HU were pulse-labeled with 5-iodo-2′-deoxyuridine (IdU, red) and subsequently released into fresh media containing only 5-chloro-2′-deoxyuridine (CldU, green) (Fig. 6D, left). We observed approximately 14.3 and 12.9% of collapsed forks in *wt* and *brl2-5A* cells, respectively, under HU treatment, while *brl2-5D* cells exhibited around 8.2% of collapsed forks. In HU-treated $cds1^{Chk2}\Delta$ and *brl2-5A* $cds1^{Chk2}\Delta$ cells, the rate of collapsed forks increased to approximately 44.8 and

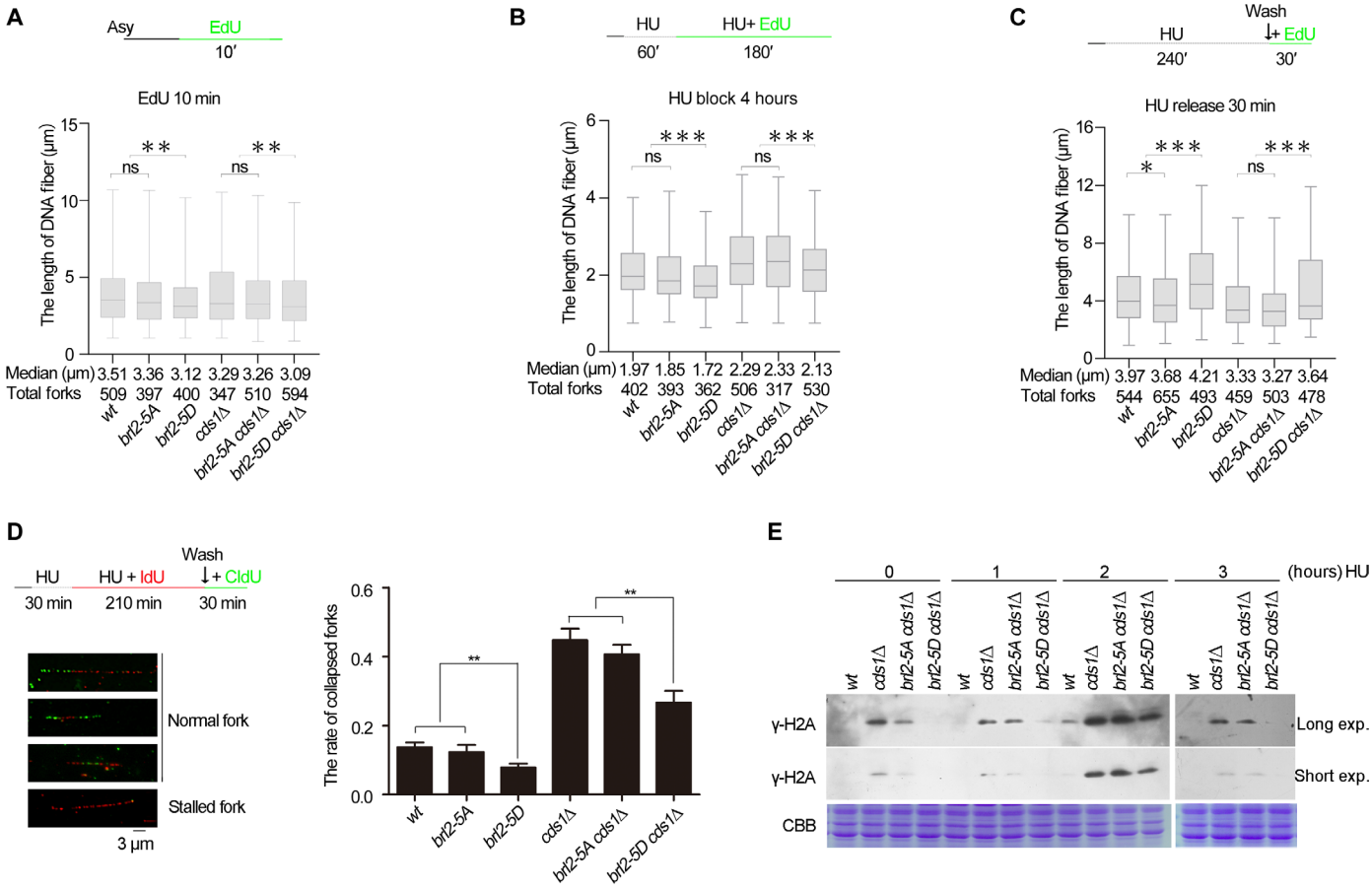

Fig. 6. The phosphomimic mutation *brl2-5D* promotes replication fork stability under HU stress. (**A**) The medium length of 5-ethynyl-2′-deoxyuridine (EdU)–labeled DNA fibers in the *wt* and indicated mutant strains under normal cell growth conditions. (**B** and **C**) The medium length of EdU-labeled DNA fibers in the *wt* and indicated mutant strains in the presence of HU and after release from HU treatment. The number of measured DNA fibers is indicated. (**D**) Dual labeling combing to assess the rate of stalled fork collapse. Left: Schematic of the single-molecule DNA fiber tract analysis for replication fork collapse frequency and the representative IdU tracks (red) during HU block and CldU tracks (green) after HU release. Right: Replication fork collapsed histogram was calculated as the single red DNA fibers divided by all of the fibers containing red signaling. At least 300 fibers were counted in each sample. Statistical test used was the Student's two-tailed *t* test, and the *P* value is indicated by asterisks (**$P < 0.005$ and ***$P < 0.001$). (**E**) The *brl2-5D* decreased the γ-H2A signal in HU-treated *cds1*^{Chk2}Δ cells. The indicated cells were grown to semi-log phase [optical density at 600 nm (OD_{600}) = 0.4], treated with 12.5 mM HU at 30°C, and harvested at the indicated time points. WCEs from cells were resolved by SDS-PAGE and analyzed by Western blot analysis using antibody against γ-H2A. ns, not significant.

40.6%, respectively, whereas *brl2-5D cds1*^{Chk2}Δ cells showed an increase to about 27.1% (Fig. 6D, right). These findings suggest that the phospho-mimic mutation *brl2-5D* effectively prevents the collapse of stalled forks in both *wt* and *cds1*^{Chk2}Δ backgrounds. Furthermore, the similar rate of collapsed forks observed in *cds1*^{Chk2}Δ and *brl2-5A cds1*^{Chk2}Δ cells supports the conclusion that Cds1^{Chk2} and Brl2 function within the same pathway.

As an additional marker of replication fork collapse, we examined the level of H2A phosphorylation at serine 139 (γ-H2A), which is associated with double-strand DNA breaks. Western blot analysis revealed that deletion of *cds1*^{Chk2} or the combination of *brl2-5A* with *cds1*^{Chk2}Δ results in up-regulation of γ-H2A levels under unperturbed conditions; however, no noticeable γ-H2A signal was detected in *wt* and *brl2-5D cds1*^{Chk2}Δ cells. Following treatment with 12.5 mM HU for 2 hours, the γ-H2A signal peaked and then decreased. Notably, γ-H2A accumulation was lower in *brl2-5D cds1*^{Chk2}Δ cells compared to *cds1*^{Chk2}Δ and *brl2-5A cds1*^{Chk2}Δ cells at all time points (Fig. 6E). These results suggest that *brl2-5D* reduces DNA damage in *cds1*^{Chk2}Δ cells, both in the absence and presence of HU, consistent with the enhanced HU resistance observed in *brl2-5D cds1*^{Chk2}Δ cells compared to *cds1*^{Chk2}Δ cells.

brl2-5D preserves the integrity of the replisome

To investigate the mechanism by which *brl2-5D* prevents stalled replication forks from collapsing, we examined the coupling of the replicative helicase CMG complex and DNA polymerases in *wt*, *cds1*^{Chk2}Δ, and *cds1*^{Chk2}Δ *brl2-5D* cells. HU-arrested replication forks were isolated using an anti-Myc antibody against Myc-tagged RPA, and the levels of DNA polymerases α and δ, the Mcm7 subunit, Cdc45, and other replisome components were quantified. Western blot analysis revealed that the amounts of DNA polymerase δ (Pol3 subunit) and DNA polymerase α (Spb70 subunit) were similar in *wt*, *cds1*^{Chk2}Δ, and *cds1*^{Chk2}Δ *brl2-5D* cells, indicating their retention at the stalled replication forks. In contrast, the amount of

CMG helicase (Mcm7 subunit) was reduced by approximately 36% in *cds1*^{Chk2}Δ cells compared to *wt* cells, suggesting that the CMG helicase dissociated from about 36% of stalled replication forks. In *cds1*^{Chk2}Δ *brl2-5D* cells, only around 21% of the CMG helicase (Mcm7 subunit) moved away from stalled replication forks. Regarding the Cdc45 subunit, another component of the CMG complex, its dissociation pattern mirrored that of the Mcm7 subunit, with approximately 38 and 20% of the Cdc45 subunit dissociating from stalled replication forks in *cds1*^{Chk2}Δ and *cds1*^{Chk2}Δ *brl2-5D* cells, respectively (Fig. 7A). Like DNA polymerases α and δ, the levels of RPA (Ssb1 subunit, tagged with 3Myc) were comparable among *wt*, *cds1*^{Chk2}Δ, and *cds1*^{Chk2}Δ *brl2-5D* cells. Because of the poor growth of *htb1-K119R* cells, we were unable to assess the uncoupling rate of the CMG helicase and DNA polymerases in this background. These results suggest that by inhibiting the uncoupling of the CMG helicase and DNA polymerases, *brl2-5D* stabilizes stalled replication forks.

Through Cds1^{Chk2}-mediated phosphorylation of Brl2, the level of H2Bub1 markedly decreases (Figs. 2, C and D, 4, B to D, and 5F), leading to considerable chromatin condensation that prevents the uncoupling of the CMG replicative complex and DNA polymerases, thereby stabilizing stalled replication forks (Fig. 7A). To evaluate the relationship between *brl2-5D* and *htb1-K119R* cells at the chromatin level, we examined chromatin condensation through MNase digestion in these cell lines. Notably, chromatin condensation is markedly greater at the whole chromatin level in *htb1-K119R* cells compared to *wt* cells, as the chromatin in *htb1-K119R* cells exhibited increased resistance to MNase digestion (Fig. 7B, right and left), indicating the critical role of H2BK119 deubiquitination in regulating chromatin condensation. A direct comparison of chromatin condensation levels between *brl2-5D* and *htb1-K119R* cells showed that chromatin condensation was similar in both cell types yet markedly higher than in *wt* and *brl2-5A* cells (Fig. 7C, right and left). Given that a low H2Bub1 level is essential for heterochromatin formation and maintenance (*65*), these findings suggest that checkpoint regulation, akin to chromsfork control (*8*), plays a crucial role in the formation of heterochromatin and compacted chromatin domains.

DISCUSSION

This study elucidates that nucleosomes serve as pivotal targets for the intra-S phase checkpoint in response to replication stress, particularly during replication fork stalling. Through the phosphorylation of the ubiquitin E3 ligase Brl2 by Cds1^{Chk2} kinase (Fig. 4, B to D), the enzymatic activity of Brl2 is markedly diminished or entirely abrogated (Fig. 5G). This reduction leads to a marked decrease in the levels of H2BK119ub1 within the chromatin surrounding stalled replication forks (Fig. 5, F to I), consequently resulting in substantial chromatin compaction at these sites (Fig. 7, B and C). Such compaction inhibits the translocation of the replicative helicase CMG complex away from stalled replication forks, thereby maintaining the biochemical and physical linkage between the replicative helicase and DNA polymerases, which stabilizes these stalled forks (Fig. 7, A and D). Furthermore, this investigation highlights the critical function of the intra-S phase checkpoint in the establishment of fundamental chromatin structures, including the formation of heterochromatin or compact chromatin domains at sites of replication fork stalling. H2BK119ub1 in fission yeast, along with its counterparts H2BK123 and H2BK120 in budding yeast and human cells, respectively, serves as a characteristic histone modification associated with euchromatin and active transcription (*69*, *70*). In contrast, a low level of H2BK123ub1, H2BK119ub1, or H2BK120ub1—alongside the deubiquitination of H2BK119, H2BK123, and H2BK120—is requisite for the assembly of heterochromatin or compacted chromatin in budding yeast, fission yeast, and human cells (*65*, *66*, *71*). Given the profound impact of chromatin structures on various biological processes, including gene transcription, DNA replication, recombination, lesion repair, and genome stability, the essential role of the ATR and Chk1-mediated intra-S phase checkpoint in the formation of heterochromatin or compacted chromatin may elucidate why ATR and Chk1 are critical for cell proliferation and embryonic development, in contrast to ATM (*46*, *49*).

H2BK123 in budding yeast corresponds to H2BK119 in *S. pombe*. A previous study revealed that the histone chaperone FACT (facilitates chromatin transcription) enhances the activity of the Ubp10 deubiquitinase on nucleosomes, specifically leading to the deubiquitination of H2BK123 (*72*). Consequently, an increase in H2B-ub1 levels was observed in FACT mutant strains (*72*). Cells with a genetic background involving a FACT mutation or Ubp10 deletion exhibited greater sensitivity to HU than *wt* cells (*72*). This finding implies that elevated levels of H2BK123 ubiquitination negatively affect HU-induced replication stress. In a related study, the accumulation of H2B-ub1 was achieved through the overexpression of an H2B-linker-ub1 fusion protein, where a ubiquitin molecule was tagged at the C terminus of H2B, thereby mimicking the accumulation of H2BK123 ubiquitination due to its resistance to deubiquitination. Cells overexpressing the H2B-linker-ub1 fusion protein also displayed heightened sensitivity to HU (*73*), and the recovery of replication forks from HU-induced arrest was markedly delayed in this strain (*73*). These two studies collectively suggest that high levels of H2BK123 ubiquitination in budding yeast have detrimental effects on HU-induced replication stress, contributing to the destabilization of stalled replication forks. The observations in budding yeast substantiate the current finding that the intra-S phase checkpoint regulates the E3 ligase Brl2 to reduce the levels of H2BK119ub1, thereby stabilizing stalled replication forks (Fig. 7D).

In addition to Brl2, the intra-S phase checkpoint likely regulates a group of enzymes that modulate histone modifications, contributing to chromatin compaction and the stability of stalled replication forks. These enzymes may include histone deacetylases, methyltransferases, ubiquitin ligases, and deubiquitinases, among others. They primarily act on histone proteins within nucleosomes, chemically modifying them. Under conditions of replication stress or fork stalling, the intra-S phase checkpoint kinase ATR or Chk2 (Chk1 in metazoan cells) phosphorylates these enzymes, altering their enzymatic activities, which leads to changes in histone modifications, resulting in enhanced chromatin compaction. Compacted chromatin prevents the physical separation of the replicative helicase and DNA polymerases, thereby preserving replisome integrity at stalled replication forks. In addition to the aforementioned enzymes, histone chaperones and chromatin remodeling complexes may also be targets of the intra-S phase checkpoint. Over the next 5 to 10 years, identifying these checkpoint targets is anticipated to be a major focus in the field of cellular regulation and the stability of stalled replication forks, including elucidating how the checkpoint regulates these targets.

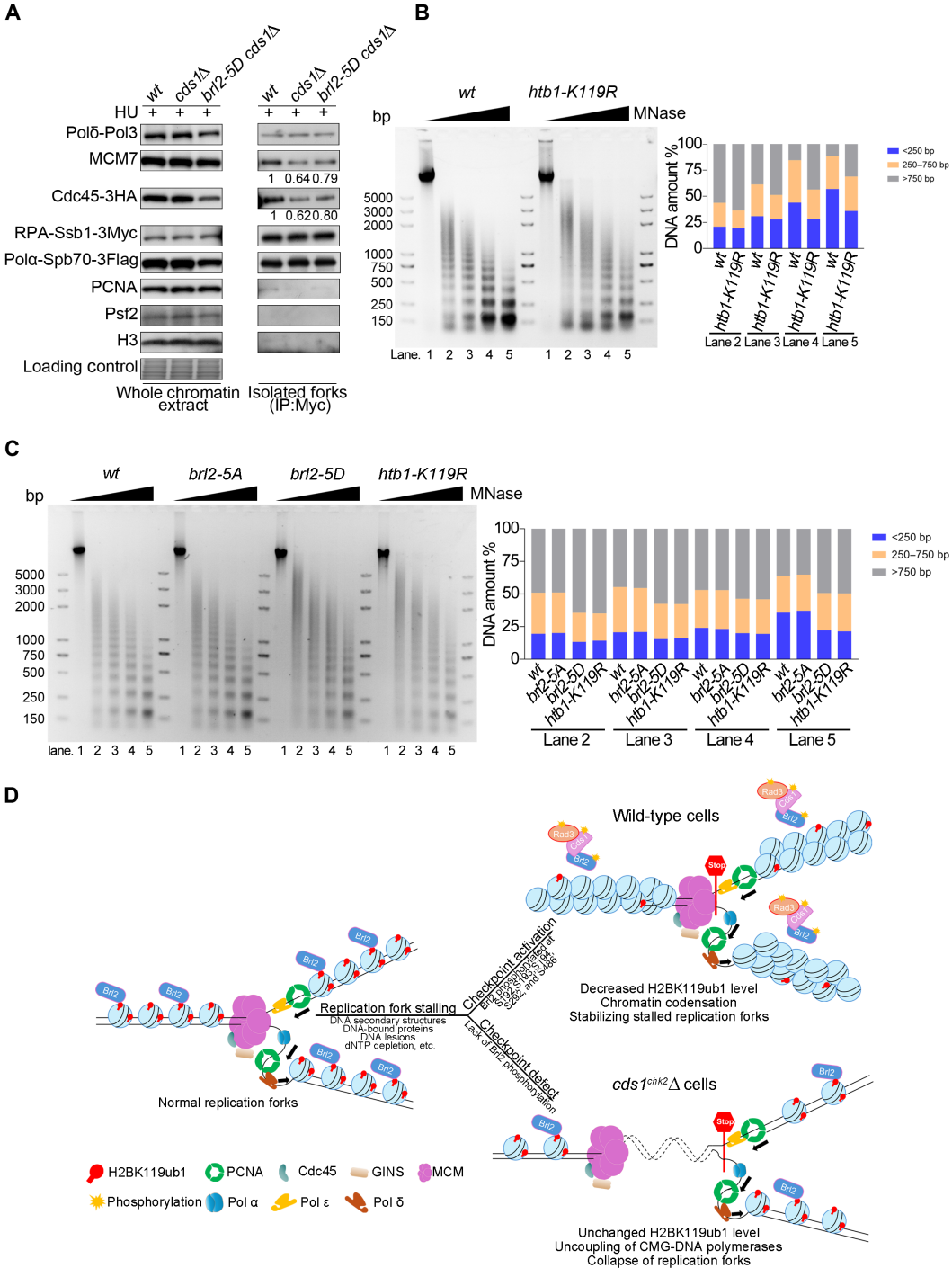

Fig. 7. Chromatin condensation promoted by Cds1^{Chk2}-mediated Brl2 phosphorylation prevents the separation of the replication helicase CMG complex from DNA polymerase α or δ. (**A**) The phosphomimic *brl2-5D* mutant prevents the separation of the CMG helicase from DNA polymerases at stalled replication forks. The cells were treated with HU for 3 hours. Formaldehyde cross-linked chromatin was isolated and sonicated to an average size of ~700 bp. Replication forks were isolated by ChIP with monoclonal anti-Myc antibody against RPA-Ssb1-3Myc. The levels of PolΔ-Pol3, MCM7, Cdc45-3HA, Polα-Spb70-3FLAG, RPA-Ssb1-3Myc, and the indicated proteins in chromatin or isolated replication forks were measured with the corresponding specific antibody. (**B**) Left: MNase digestion of chromatin in *wt* and *htb1-K119R* cells. Right: Analysis of relative percentage of different sizes of DNA fragments. (**C**) Left: MNase digestion of chromatin in *wt*, *brl2-5A*, *brl2-5D*, and *htb1-K119R* cells. Right: Analysis of relative percentage of different sizes of DNA fragments. (**D**) Diagram of the regulation of ubiquitin E3 ligase Brl2 by the intra-S checkpoint pathway to stabilize stalled replication forks. The stalling of the replication fork activates the checkpoint kinase Cds1^{Chk2}. Then, Cds1^{Chk2} phosphorylates Brl2 at S192, S193, S194, S292, and S486, resulting in a sharp reduction of the H2Bk119ub1 level, which markedly enhances chromatin condensation. Condensed chromatin prevents the uncoupling of the replicative helicase CMG complex from DNA polymerases, which stabilizes stalling replication forks. Black arrow: direction of leading and lagging strand DNA synthesis. dNTP, deoxynucleoside triphosphate.

This study provides critical evidence linking the stalling of replication forks to the intra-S phase checkpoint–regulated formation of heterochromatin and compacted chromatin domains. In fission yeast, the ubiquitination of H2BK119, along with the corresponding modifications in budding yeast and metazoan cells, serves as a hallmark of euchromatin and active transcription (*74*–*76*). Conversely, a low level of ubiquitination at the H2BK119, H2BK123, or H2BK120 site in fission yeast, budding yeast, or human cells is necessary for the assembly of heterochromatin (*65*, *66*, *71*). This study demonstrates that the intra-S phase checkpoint considerably reduces the level of H2BK119ub1 in response to replication stress, thus promoting the formation of heterochromatin and compacted chromatin domains at sites of replication fork stalling. A previous study has reported that chromatin compaction induced by H2BK33 deacetylation and H3K9 trimethylation occurs at replication fork stalling sites in fission yeast (*8*). Furthermore, it suggests that H2BK33 deacetylation and H3K9 trimethylation are regulated by chromsfork control rather than the checkpoint (*8*). However, recent findings indicate that the intra-S phase checkpoint may contribute to the increased levels of H3K9me3 at stalled replication fork sites in human cells (*77*). It remains to be clarified whether H3K9 trimethylation at stalled replication fork sites is regulated by different mechanisms, whether chromsfork control or the intra-S phase checkpoint, in various species. At the molecular level, this study convincingly demonstrates that the intra-S phase checkpoint plays a crucial role in the formation of heterochromatin and compacted chromatin domains at replication fork stalling sites (Fig. 7D). Future research will deepen our mechanistic understanding of these two vital biological events: (i) how the intra-S phase checkpoint regulates the stabilization of stalled replication forks, and (ii) how the assembly of heterochromatin or compacted chromatin domains occurs at replication fork stalling sites.

MATERIALS AND METHODS

Yeast strains, plasmids, and genetic manipulation

The fission yeast *S. pombe* strains used in this study and their relevant genotypes are listed in table S1. The *S. pombe* strain FY11064 was purchased from National BioResource Project–Yeast (https://yeast.nig.ac.jp/yeast/). Strain construction was based on the gene replacement technique of Scherer and Davis (*78*). The plasmids used for gene editing experiments were derived from pBluescript, pFA6a-kanMX6, and pSLF1072 as described elsewhere (Addgene, Watertown, MA, USA). Site-directed mutations of *brl2* gene were introduced using the QuikChange Site-Directed Mutagenesis Kit (Stratagene, La Jolla, CA, USA), following the protocol provided by the manufacturer. Yeast transformations were performed using the lithium acetate method. Cells were cultured in YES-rich medium [yeast extract (5 g/liter) and glucose (30 g/liter), supplemented with adenine (250 mg/liter), uracil (250 mg/liter), histidine (250 mg/liter), and leucine (250 mg/liter)] or Edinburgh minimal medium (EMM), supplemented with adenine (250 mg/liter), histidine (250 mg/liter), and leucine (250 mg/liter) or EHAL medium [EMM medium supplemented with histidine (250 mg/liter), adenine (250 mg/liter), and leucine (250 mg/liter)]. For the plate-based spot assay, cells in log-phase growth were serially diluted fivefold and spotted onto the indicated plates containing no drug or the indicated HU concentration. The plates were incubated for 3 to 5 days at 30°C and photographed.

Preparation of whole cell extract and immunoblotting

The whole cell extracts were prepared essentially as described previously with some minor changes (*79*). About 2×10^8 cells were collected and frozen quickly in liquid nitrogen for 10 min. Cells were washed with 500 μl of 20% trichloroacetic acid (TCA) once and resuspended in 500 μl of 20% TCA, and then 500 μl of acid-washed glass beads (G8772; MilliporeSigma, Burlington, MA, USA) was added. The cells were disrupted by vortexing for 8 min at room temperature. Beads were separated and washed with 1 ml of 5% TCA buffer. The resulting extracts were centrifuged for 10 min at 13,000 rpm at room temperature. The pellet was resuspended in 60 μl of 2× SDS loading buffer and 30 μl of 1 M tris to neutralize TCA, boiled for 5 min, and centrifuged for 10 min at 3000 rpm at room temperature. The supernatant was divided into aliquots and stored at −80°C. About 5 to 10 μl of sample was analyzed by SDS–polyacrylamide gel electrophoresis (SDS-PAGE) followed by immunoblot analysis using the indicated antibodies. For the dot blots, 2 μl of the indicated amounts of Brl2 peptides was spotted on 0.2-μm polyvinylidene difluoride membranes and detected using the corresponding phosphorylated antibodies. The antibodies used in Western blot analysis are antibodies against H2B (in lab), hemagglutinin (HA; in lab), H2BK120ub1 (05-1312; MilliporeSigma), H3 (BE3015; EASYBIO, Beijing, China), γH2A (ab17353; Abcam, Cambridge, UK), single-strand DNA binding (SSB) protein (in lab), Brl2 (in lab), phosphor-Brl2 (pS292) (in lab), phosphor-Brl2 (pS486) (in lab), and phosphor-Brl2 (pS192/193/194) (in lab). Phos-tag acrylamide (25 μM; Boppard, Shanghai, China) and 6% gel concentration were used in our experiments.

Chromatin purification

For chromatin purification, the cells were grown to log-phase in liquid YES medium, harvested by centrifugation, and washed once with the stop buffer containing 20 mM tris-HCl (pH 7.5), 150 mM NaCl, 50 mM NaF, 10 mM EDTA, and 1 mM NaN_3. The yeast cell wall was digested in sorbitol buffer [1.2 M sorbitol, 10 mM dithiothreitol (DTT), 20 mM EDTA, lysing enzyme (1 mg/ml; L1412, MilliporeSigma), and appropriate lyticase (L4025; MilliporeSigma)] at 30°C for 40 to 60 min. When ~90% cells were "ghost" in 1% Triton X-100, the spheroplasts were washed twice with precooled 1.2 M sorbitol containing 1 mM phenylmethylsulfonyl fluoride (PMSF) and then lysed in buffer A [50 mM tris-HCl (pH 7.5), 100 mM KCl, 5 mM $MgCl_2$, 2 mM EDTA, 10% glycerol, 0.05% NP-40, 1 mM PMSF, pepstatin (1 μg/ml), leupeptin (1 μg/ml), aprotinin (1 μg/ml), and 5 μM of the cell-permeable proteasome inhibitor MG132] containing 1% Triton X-100. The chromatin fraction was isolated by high-speed centrifugation at 4°C, 18,000 rpm for 20 min and washed twice with buffer A. The pellet was resuspended in 1× SDS loading buffer and boiled at 95°C for 5 min to release the chromatin-enriched proteins.

Protein purification

To facilitate Brl2 purification, we first integrated the C-terminal 8his-3HA–tagged *brl2* cassette into the yeast *brl2* locus (*80*). The resulting *brl2-8his-3HA* strain can express Brl2-8His-3HA protein under the control of the *brl2* native promoter. The *brl2-8his-3HA* cells, with or without HU treatment for 3 hours, were harvested at log phase, washed once with the precooled lysis buffer [20 mM tris-HCl (pH 7.5), 100 mM KCl, 0.05% Triton X-100, 50 mM NaF, 1 mM Na_3VO_4, 1 mM PMSF, pepstatin (1 μg/ml), leupeptin (1 μg/ml),

aprotinin (1 μg/ml), and 5 μM MG132], and resuspended in the lysis buffer containing 5 mM imidazole. The subsequent procedures were all performed at 4°C. Cells were disrupted with an equal volume of acid-washed glass beads. The lysate was centrifuged at 18,000 rpm for 30 min. The supernatants were filtered through a 0.45-μm membrane and loaded on Ni-NTA (nickel–nitrilotriacetic acid) resin column (Qiagen GmbH, Hilden, Germany), pre-equilibrated with the lysis buffer containing 5 mM imidazole. The bound protein was washed with 4× bed volume lysis buffer containing 50 mM imidazole. The Brl2-8his-3HA was eluted from the beads with 200 mM imidazole, and the fraction containing the Brl2-8his-3HA was subjected to HA affinity chromatography with 30 μl of HA beads (A2095; MilliporeSigma). After rotation for 3 hours, the beads were washed three times with lysis buffer. The enriched Brl2-8His-3HA protein on HA beads were released with either HA peptide to obtain biologically active Brl2 or by boiling at 95°C for 5 min in 1× SDS loading buffer and then separating by 10% SDS-PAGE.

Cds1-SSB-6his was overexpressed under the control of an exogenous *nmt1* promoter. The cells containing an integrated *pSLF1072 nmt1::cds1-ssb-6his* plasmid were cultured at 30°C in EMM containing thiamine (5 μg/ml) to repress the *nmt1* promoter. To induce overexpression of Cds1, thiamine was removed 12 hours before adding HU (1 M stock diluted to 12.5 mM final concentration) for activating the intra-S checkpoint pathway and stimulating Cds1 activity. After incubation for 3 hours at 30°C, the cells were harvested, washed once with above lysis buffer, and resuspended in lysis buffer. The cells were lysed with acid-washed glass beads, and the protein crude extracts were obtained after centrifugation at 4°C, 18,000 rpm for 30 min. The Cds1-SSB-6his was purified by ammonium sulfate precipitation and Ni-NTA column chromatography as the standard method. Protein precipitation was performed by progressively adding ammonium sulfate from 0 to 20% and then 20 to 50% for Cds1-SSB-6his, which was eluted from the Ni-NTA column with buffer containing 200 mM imidazole. Eventually, the fraction containing Cds1-SSB-6his was dialyzed against buffer containing 25 mM tris-HCl (pH 7.5), 100 mM NaCl, 10% glycerol, 1 mM PMSF, pepstatin (1 μg/ml), leupeptin (1 μg/ml), and aprotinin (1 μg/ml) and stored at −80°C for subsequent analysis.

Phosphorylation assay of Brl2 in vitro and MS analysis of Brl2 phosphorylated sites

For in vitro phosphorylation assay of Brl2 by Cds1, the Brl2-8his-3HA protein was purified from 2 liters of culture and enriched by Ni-NTA column chromatography and HA beads as described above, but no phosphatase inhibitors (50 mM NaF and 1 mM Na_3VO_4) were added during the purification process. Brl2-8his-3HA–bound HA beads were split, and 20 pmol of purified Cds1-SSB-6his was added to half of it. Phosphorylation reaction was incubated for 30 min at 37°C in 20 μl of kinase buffer [20 mM Hepes (pH 7.5), 10 mM $MgCl_2$, 150 mM KCl, 1 mM EDTA, and 4 mM ATP]. The reaction was stopped by washing the beads three times with washing buffer [20 mM tris-HCl (pH 7.5), 100 mM KCl, 50 mM NaF, 1 mM Na_3VO_4, 1 mM PMSF, pepstatin (1 μg/ml), leupeptin (2 μg/ml), and aprotinin (2 μg/ml)]. The Brl2-8his-3HA was released from HA beads with 1× SDS loading buffer and then resolved on a 10% SDS-PAGE gel or a 6% Phos-tag gel containing 25 μM Phos-tag. Polyclonal anti-Brl2 was used to detect Brl2 and phosphorylated Brl2. For MS analysis, the obtained Brl2-8his-3HA protein was phosphorylated in vivo or in vitro. For the in vivo assay, HU was added at 12.5 mM final concentration in the culture for 4 hours to activate the intra-S checkpoint pathway kinases that phosphorylate Brl2-8his-3HA, and after harvesting the cells, Brl2-8his-3HA was purified as described above. For the in vitro assay, the purified Brl2-8his-3HA was phosphorylated by Cds1-SSB-6his in an in vitro phosphorylation reaction. Ultimately, the phosphorylated Brl2-8his-3HA was separated on a 10% SDS-PAGE gel. The band containing Brl2 was visualized by Coomassie brilliant blue staining and cut out for MS analysis using standard protocols.

Preparation and purification of antibodies against phosphorylated Brl2

Antigen peptides of 10 to 15 amino acids in length were synthesized by adding keyhole limpet hemocyanin (KLH) at its C terminal to produce immunogenicity. These peptide-KLHs were used to immunize rabbits, and the crude serum containing a polyclonal antipeptide antibody was collected (*81*, *82*). Briefly, modified and unmodified Brl2 peptides were separately cross-linked to the CNBr-activated Sepharose 4B resin (#GE17-0756-01; GE Healthcare Life Sciences Inc., Piscataway, NJ, USA) to prepare the peptide affinity columns. The serum was diluted fourfold with phosphate-buffered saline (PBS) and loaded onto the Brl2 phosphorylated peptide affinity column. After washing with PBS, the antibodies were eluted with acidic elution buffer [50 mM glycine-HCl (pH 3.0), 0.1% Triton X-100, and 0.15 M NaCl] and collected in a tube with $^1/_{10}$ volume of 1 M tris-HCl to neutralize the buffer. Then, the eluate was applied to the unmodified Brl2 peptide affinity column. The antibodies that recognize nonphosphorylated peptides would stick to the column, and the antibodies that recognize phosphorylated peptides would flow through. This flow through fraction was collected and dialyzed against PBS buffer. The resulting antibodies recognizing phosphorylated Brl2 were resuspended in PBS containing 50% glycerol and stored at −20°C.

Chromatin immunoprecipitation and quantitative polymerase chain reaction

ChIP of fission yeast cells was performed as described with several modifications (*83*). The cells were cross-linked with 1% formaldehyde for 20 min at room temperature and quenched with 125 mM glycine for 5 min. Chromatin was obtained as described above and sonicated using a BioRuptor Pico sonicator (JY92-IIN; Diagenode Inc., Denville, NJ, USA) to generate DNA fragments with a mean length of 300 to 700 bp, followed by centrifugation twice at 4°C, 15,000 rpm for 10 min. The resultant supernatants were precleared with protein A beads (SE251005; Thermo Fisher Scientific Inc., Waltham, MA, USA) at 4°C for 1 hour. After saving back 10% of the total supernatant for use as the input sample, the rest was incubated with 2 μg of the appropriate antibody overnight at 4°C. Immune complexes were mixed with ChIP-Grade Protein A/G Plus Agarose (QJ223903; Thermo Fisher Scientific Inc.) for 1 hour at 4°C and washed rigorously. Then, the chromatin immunoprecipitated on the beads were eluted with TES buffer [20 mM tris-HCl (pH 8.0), 10 mM EDTA, and 1% SDS] for 40 min at 65°C. The collected material and input sample with 1% SDS were incubated at 65°C for 2 hours to reverse cross-linking and then treated with ribonuclease A (EN0531; Thermo Fisher Scientific Inc.) for 1 hour at 37°C. Subsequently, proteinase K (P2308; MilliporeSigma) was added to continue reversing cross-linking overnight at 60°C. The DNA was purified by a Qiagen PCR purification kit (Qiagen GmbH). ChIP DNA was quantitated

using the Hieff qPCR SYBR Green Master Mix (11201ES08; Yeasen Biotech, Shanghai, China), and qPCR was performed using a Roche LightCycler 96 Real-Time PCR System (Roche Diagnostics GmbH, Mannheim, Germany). ChIP-qPCR primer sequences are listed in table S2.

DNA combing analysis and microscopy imaging

DNA combing analysis was performed as previously described (*84*). The strain J2172, which coexpresses the *Herpes simplex* virus thymidine kinase gene (*hsv-tk*) and a human equilibrative nucleoside transporter (*hENT1*), was used for DNA combing analysis. The cells were labeled with 2.5 μM IdU (I7125; MilliporeSigma) and CldU (200 μg/ml; C6891; MilliporeSigma). Following incorporation, the reaction in cells was stopped by the addition of sodium azide at 3 mM final concentration on ice. Three minutes later, cells were harvested and concentrated to 50 optical density (OD)/ml in a buffer containing 1.2 M sorbitol and 50 mM EDTA. Afterward, cells were mixed with an equal volume of 1.3% molten low-melting point agarose (42°C). The cell suspension was transferred to a plug mold to generate genomic DNA plugs. Solidified plugs were incubated overnight at 37°C in lyticase buffer (1.2 M sorbitol, 50 mM EDTA, 10 mM DTT, appropriate lysing enzyme, and lyticase) to digest the cell wall. Then, plugs were washed three times in proteinase K buffer [proteinase K (2 mg/ml), 10 mM tris-HCl (pH 7.5), and 50 mM EDTA] and incubated for 48 hours at 42°C in proteinase K buffer. Plugs were washed five times in 5 ml of TE_{50} buffer [10 mM tris-HCl (pH 7.5) and 50 mM EDTA]. Subsequently, plugs were washed three times with 5 ml of TE buffer [10 mM tris (pH 7.5) and 1 mM EDTA] and then incubated in 2 ml of 50 mM MES buffer at pH 5.7 for 10 min. After melting the plugs fresh MES buffer at 65°C for 10 min, they were allowed to settle at 42°C adding 3 U of β-agarose I (M0392S; New England Biolabs Inc., Ipswich, MA, USA) for 4 hours or overnight. Afterward, the DNA solution was incubated for 10 min at 65°C and for 10 min at room temperature for DNA combing analysis. DNA solution was dipped on silanized coverslips (COV-001; Genomic Vision SA, Bagneux, France) and pulled out at a constant speed with a pull machine. Then, the coverslips were cross-linked at 60°C for 3 hours or overnight in the dark. The coverslips were stored at −20°C until use.

The DNA fibers labeled with IdU and CldU were denatured in 1 M NaOH for 22 min for immunostaining with the indicated antibodies: IdU (347580; BD Biosciences, Franklin Lakes, NJ, USA) and CldU (C188215; Lifespan Bioscience, Lynnwood, WA, USA). The cells were imaged on a Delta Vision Elite microscope (Applied Precision, Uppsala, Sweden), using a 60× oil lens, and images were analyzed using the Volocity software (PerkinElmer, Waltham, MA, USA). A minimum of 300 fibers per sample were imaged.

MNase digestion

Yeast cultures from *wt*, *brl2-5A*, *brl2-5D*, and *htb1-K119R* (about 300 OD for each strain) were harvested and washed twice with ice-cold water. Cell pellets were resuspended in 5 ml of lysis buffer [1.2 M sorbitol, 10 mM DTT, lysing enzyme (0.75 mg/ml), and appropriate lyticase] and incubated in a water bath at 32°C with shaking for 40 to 60 min. Then, cells were collected by centrifugation at 4°C and washed twice with ice-cold 1.2 M sorbitol containing 1 mM PMSF. The spheroplasts were obtained in MND buffer [1.2 M sorbitol, 100 mM NaCl, 5 mM $CaCl_2$, 5 mM $MgAc_2$, 1 mM EDTA, 50 mM tris-HCl (pH 8.0), 1% Triton X-100, and 5 mM spermidine] and divided into four equal aliquots. An aliquot was set as mock digestion (0 U/ml, 0 min), and the others were treated with MNase (2400 U) with different incubation time periods at room temperature. The digestion was stopped by adding an equal volume of 2× stop buffer (50 mM EDTA and 1% SDS). The DNA was extracted twice by phenol-chloroform and once by chloroform. The DNA was resuspended in 100 μl of TE buffer [10 mM tris-HCl (pH 8.0) and 1 mM EDTA], followed by RNase digestion for 30 min at 37°C. Ultimately, the DNA was resolved in 1.5% agarose gel and stained with ethidium bromide for visualization.

Supplementary Materials

This PDF file includes:

Tables S1 and S2
Figs. S1 to S4

REFERENCES AND NOTES

1. R. D. Kornberg, Y. Lorch, Twenty-five years of the nucleosome, fundamental particle of the eukaryote chromosome. *Cell* **98**, 285–294 (1999).
2. E. Passarge, Emil Heitz and the concept of heterochromatin: Longitudinal chromosome differentiation was recognized fifty years ago. *Am. J. Hum. Genet.* **31**, 106–115 (1979).
3. R. C. Allshire, H. D. Madhani, Ten principles of heterochromatin formation and function. *Nat. Rev. Mol. Cell Biol.* **19**, 229–244 (2018).
4. B. J. Strober, R. Elorbany, K. Rhodes, N. Krishnan, K. Tayeb, A. Battle, Y. Gilad, Dynamic genetic regulation of gene expression during cellular differentiation. *Science* **364**, 1287–1290 (2019).
5. M. Cardoso-Moreira, J. Halbert, D. Valloton, B. Velten, C. Chen, Y. Shao, A. Liechti, K. Ascenção, C. Rummel, S. Ovchinnikova, P. V. Mazin, I. Xenarios, K. Harshman, M. Mort, D. N. Cooper, C. Sandi, M. J. Soares, P. G. Ferreira, S. Afonso, M. Carneiro, J. M. A. Turner, J. L. VandeBerg, A. Fallahshahroudi, P. Jensen, R. Behr, S. Lisgo, S. Lindsay, P. Khaitovich, W. Huber, J. Baker, S. Anders, Y. E. Zhang, H. Kaessmann, Gene expression across mammalian organ development. *Nature* **571**, 505–509 (2019).
6. L. Xue, H. Yi, Z. Huang, Y.-B. Shi, W.-X. Li, Global gene expression during the human organogenesis: From transcription profiles to function predictions. *Int. J. Biol. Sci.* **7**, 1068–1076 (2011).
7. B. D. Strahl, C. D. Allis, The language of covalent histone modifications. *Nature* **403**, 41–45 (2000).
8. G. Feng, Y. Yuan, Z. Li, L. Wang, B. Zhang, J. Luo, J. Ji, D. Kong, Replication fork stalling elicits chromatin compaction for the stability of stalling replication forks. *Proc. Natl. Acad. Sci. U.S.A.* **116**, 14563–14572 (2019).
9. R. Janke, G. A. King, M. Kupiec, J. Rine, Pivotal roles of PCNA loading and unloading in heterochromatin function. *Proc. Natl. Acad. Sci. U.S.A.* **115**, E2030–E2039 (2018).
10. T. Krude, C. Keller, Chromatin assembly during S phase: Contributions from histone deposition, DNA replication and the cell division cycle. *Cell. Mol. Life Sci.* **58**, 665–672 (2001).
11. S. Liu, Z. Xu, H. Leng, P. Zheng, J. Yang, K. Chen, J. Feng, Q. Li, RPA binds histone H3-H4 and functions in DNA replication-coupled nucleosome assembly. *Science* **355**, 415–420 (2017).
12. X. Li, L. Wang, X. Liu, Z. Zheng, D. Kong, Cellular regulation and stability of DNA replication forks in eukaryotic cells. *DNA Repair (Amst)* **120**, 103418 (2022).
13. A. Costa, I. Ilves, N. Tamberg, T. Petojevic, E. Nogales, M. R. Botchan, J. M. Berger, The structural basis for MCM2-7 helicase activation by GINS and Cdc45. *Nat. Struct. Mol. Biol.* **18**, 471–477 (2011).
14. Z. F. Pursell, I. Isoz, E.-B. Lundström, E. Johansson, T. A. Kunkel, Yeast DNA polymerase epsilon participates in leading-strand DNA replication. *Science* **317**, 127–130 (2007).
15. H. Lou, M. Komata, Y. Katou, Z. Guan, C. C. Reis, M. Budd, K. Shirahige, J. L. Campbell, Mrc1 and DNA polymerase ε function together in linking DNA replication and the S phase checkpoint. *Mol. Cell* **32**, 106–117 (2008).
16. A. C. Simon, J. C. Zhou, R. L. Perera, F. van Deursen, C. Evrin, M. E. Ivanova, M. L. Kilkenny, L. Renault, S. Kjaer, D. Matak-Vinković, K. Labib, A. Costa, L. Pellegrini, A Ctf4 trimer couples the CMG helicase to DNA polymerase α in the eukaryotic replisome. *Nature* **510**, 293–297 (2014).
17. Y. Liu, L. Wang, X. Xu, Y. Yuan, B. Zhang, Z. Li, Y. Xie, R. Yan, Z. Zheng, J. Ji, J. M. Murray, A. M. Carr, D. Kong, The intra-S phase checkpoint directly regulates replication elongation to preserve the integrity of stalled replisomes. *Proc. Natl. Acad. Sci. U.S.A.* **118**, e2019183118 (2021).
18. J. Z. Torres, S. L. Schnakenberg, V. A. Zakian, *Saccharomyces cerevisiae* Rrm3p DNA helicase promotes genome integrity by preventing replication fork stalling: Viability of

rrm3 cells requires the intra-S-phase checkpoint and fork restart activities. *Mol. Cell. Biol.* **24**, 3198–3212 (2004).
19. V. S. Chambers, G. Marsico, J. M. Boutell, M. Di Antonio, G. P. Smith, S. Balasubramanian, High-throughput sequencing of DNA G-quadruplex structures in the human genome. *Nat. Biotechnol.* **33**, 877–881 (2015).
20. E. S. Lander, L. M. Linton, B. Birren, C. Nusbaum, M. C. Zody, J. Baldwin, K. Devon, K. Dewar, M. Doyle, W. FitzHugh, R. Funke, D. Gage, K. Harris, A. Heaford, J. Howland, L. Kann, J. Lehoczky, R. LeVine, P. McEwan, K. McKernan, J. Meldrim, J. P. Mesirov, C. Miranda, W. Morris, J. Naylor, C. Raymond, M. Rosetti, R. Santos, A. Sheridan, C. Sougnez, Y. Stange-Thomann, N. Stojanovic, A. Subramanian, D. Wyman, J. Rogers, J. Sulston, R. Ainscough, S. Beck, D. Bentley, J. Burton, C. Clee, N. Carter, A. Coulson, R. Deadman, P. Deloukas, A. Dunham, I. Dunham, R. Durbin, L. French, D. Grafham, S. Gregory, T. Hubbard, S. Humphray, A. Hunt, M. Jones, C. Lloyd, A. McMurray, L. Matthews, S. Mercer, S. Milne, J. C. Mullikin, A. Mungall, R. Plumb, M. Ross, R. Shownkeen, S. Sims, R. H. Waterston, R. K. Wilson, L. W. Hillier, J. D. McPherson, M. A. Marra, E. R. Mardis, L. A. Fulton, A. T. Chinwalla, K. H. Pepin, W. R. Gish, S. L. Chissoe, M. C. Wendl, K. D. Delehaunty, T. L. Miner, A. Delehaunty, J. B. Kramer, L. L. Cook, R. S. Fulton, D. L. Johnson, P. J. Minx, S. W. Clifton, T. Hawkins, E. Branscomb, P. Predki, P. Richardson, S. Wenning, T. Slezak, N. Doggett, J. F. Cheng, A. Olsen, S. Lucas, C. Elkin, E. Uberbacher, M. Frazier, R. A. Gibbs, D. M. Muzny, S. E. Scherer, J. B. Bouck, E. J. Sodergren, K. C. Worley, C. M. Rives, J. H. Gorrell, M. L. Metzker, S. L. Naylor, R. S. Kucherlapati, D. L. Nelson, G. M. Weinstock, Y. Sakaki, A. Fujiyama, M. Hattori, T. Yada, A. Toyoda, T. Itoh, C. Kawagoe, H. Watanabe, Y. Totoki, T. Taylor, J. Weissenbach, R. Heilig, W. Saurin, F. Artiguenave, P. Brottier, T. Bruls, E. Pelletier, C. Robert, P. Wincker, D. R. Smith, L. Doucette-Stamm, M. Rubenfield, K. Weinstock, H. M. Lee, J. Dubois, A. Rosenthal, M. Platzer, G. Nyakatura, S. Taudien, A. Rump, H. Yang, J. Yu, J. Wang, G. Huang, J. Gu, L. Hood, L. Rowen, A. Madan, S. Qin, R. W. Davis, N. A. Federspiel, A. P. Abola, M. J. Proctor, R. M. Myers, J. Schmutz, M. Dickson, J. Grimwood, D. R. Cox, M. V. Olson, R. Kaul, C. Raymond, N. Shimizu, K. Kawasaki, S. Minoshima, G. A. Evans, M. Athanasiou, R. Schultz, B. A. Roe, F. Chen, H. Pan, J. Ramser, H. Lehrach, R. Reinhardt, W. R. McCombie, M. de la Bastide, N. Dedhia, H. Blöcker, K. Hornischer, G. Nordsiek, R. Agarwala, L. Aravind, J. A. Bailey, A. Bateman, S. Batzoglou, E. Birney, P. Bork, D. G. Brown, C. B. Burge, L. Cerutti, H. C. Chen, D. Church, M. Clamp, R. R. Copley, T. Doerks, S. R. Eddy, E. E. Eichler, T. S. Furey, J. Galagan, J. G. Gilbert, C. Harmon, Y. Hayashizaki, D. Haussler, H. Hermjakob, K. Hokamp, W. Jang, L. S. Johnson, T. A. Jones, S. Kasif, A. Kaspryzk, S. Kennedy, W. J. Kent, P. Kitts, E. V. Koonin, I. Korf, D. Kulp, D. Lancet, T. M. Lowe, A. McLysaght, T. Mikkelsen, J. V. Moran, N. Mulder, V. J. Pollara, C. P. Ponting, G. Schuler, J. Schultz, G. Slater, A. F. Smit, E. Stupka, J. Szustakowki, D. Thierry-Mieg, J. Thierry-Mieg, L. Wagner, J. Wallis, R. Wheeler, A. Williams, Y. I. Wolf, K. H. Wolfe, S. P. Yang, R. F. Yeh, F. Collins, M. S. Guyer, J. Peterson, A. Felsenfeld, K. A. Wetterstrand, A. Patrinos, M. J. Morgan, P. de Jong, J. J. Catanese, K. Osoegawa, H. Shizuya, S. Choi, Y. J. Chen, J. Szustakowki, International Human Genome Sequencing Consortium, Initial sequencing and analysis of the human genome. *Nature* **409**, 860–921 (2001).
21. L. Gellon, S. Kaushal, J. Cebrián, M. Lahiri, S. M. Mirkin, C. H. Freudenreich, Mrc1 and Tof1 prevent fragility and instability at long CAG repeats by their fork stabilizing function. *Nucleic Acids Res.* **47**, 794–805 (2019).
22. M. M. Krasilnikova, S. M. Mirkin, Replication stalling at Friedreich's ataxia (GAA)n repeats in vivo. *Mol. Cell. Biol.* **24**, 2286–2295 (2004).
23. J. M. Sogo, M. Lopes, M. Foiani, Fork reversal and ssDNA accumulation at stalled replication forks owing to checkpoint defects. *Science* **297**, 599–602 (2002).
24. J. Hu, L. Sun, F. Shen, Y. Chen, Y. Hua, Y. Liu, M. Zhang, Y. Hu, Q. Wang, W. Xu, F. Sun, J. Ji, J. M. Murray, A. M. Carr, D. Kong, The intra-S phase checkpoint targets Dna2 to prevent stalled replication forks from reversing. *Cell* **149**, 1221–1232 (2012).
25. R. S. Cha, N. Kleckner, ATR homolog Mec1 promotes fork progression, thus averting breaks in replication slow zones. *Science* **297**, 602–606 (2002).
26. J. A. Cobb, L. Bjergbaek, K. Shimada, C. Frei, S. M. Gasser, DNA polymerase stabilization at stalled replication forks requires Mec1 and the RecQ helicase Sgs1. *EMBO J.* **22**, 4325–4336 (2003).
27. C. Lucca, F. Vanoli, C. Cotta-Ramusino, A. Pellicioli, G. Liberi, J. Haber, M. Foiani, Checkpoint-mediated control of replisome-fork association and signalling in response to replication pausing. *Oncogene* **23**, 1206–1213 (2004).
28. S. Lambert, A. Watson, D. M. Sheedy, B. Martin, A. M. Carr, Gross chromosomal rearrangements and elevated recombination at an inducible site-specific replication fork barrier. *Cell* **121**, 689–702 (2005).
29. S. Lambert, B. Froget, A. M. Carr, Arrested replication fork processing: Interplay between checkpoints and recombination. *DNA Repair (Amst)* **6**, 1042–1061 (2007).
30. J. A. Tercero, J. F. Diffley, Regulation of DNA replication fork progression through damaged DNA by the Mec1/Rad53 checkpoint. *Nature* **412**, 553–557 (2001).
31. Y. Zeng, K. C. Forbes, Z. Wu, S. Moreno, H. Piwnica-Worms, T. Enoch, Replication checkpoint requires phosphorylation of the phosphatase Cdc25 by Cds1 or Chk1. *Nature* **395**, 507–510 (1998).
32. M. N. Boddy, B. Furnari, O. Mondesert, P. Russell, Replication checkpoint enforced by kinases Cds1 and Chk1. *Science* **280**, 909–912 (1998).
33. G. Zachos, M. D. Rainey, D. A. F. Gillespie, Chk1-dependent S-M checkpoint delay in vertebrate cells is linked to maintenance of viable replication structures. *Mol. Cell. Biol.* **25**, 563–574 (2005).
34. D. Branzei, M. Foiani, The Rad53 signal transduction pathway: Replication fork stabilization, DNA repair, and adaptation. *Exp. Cell Res.* **312**, 2654–2659 (2006).
35. T. Caspari, C. Davies, A. M. Carr, Analysis of the fission yeast checkpoint Rad proteins. *Cold Spring Harb. Symp. Quant. Biol.* **65**, 451–456 (2000).
36. H. D. Lindsay, D. J. Griffiths, R. J. Edwards, P. U. Christensen, J. M. Murray, F. Osman, N. Walworth, A. M. Carr, S-phase-specific activation of Cds1 kinase defines a subpathway of the checkpoint response in *Schizosaccharomyces pombe*. *Genes Dev.* **12**, 382–395 (1998).
37. C. Santocanale, J. F. Diffley, A Mec1- and Rad53-dependent checkpoint controls late-firing origins of DNA replication. *Nature* **395**, 615–618 (1998).
38. K. Shirahige, Y. Hori, K. Shiraishi, M. Yamashita, K. Takahashi, C. Obuse, T. Tsurimoto, H. Yoshikawa, Regulation of DNA-replication origins during cell-cycle progression. *Nature* **395**, 618–621 (1998).
39. P. Zegerman, J. F. X. Diffley, Checkpoint-dependent inhibition of DNA replication initiation by Sld3 and Dbf4 phosphorylation. *Nature* **467**, 474–478 (2010).
40. J. Lopez-Mosqueda, N. L. Maas, Z. O. Jonsson, L. G. Defazio-Eli, J. Wohlschlegel, D. P. Toczyski, Damage-induced phosphorylation of Sld3 is important to block late origin firing. *Nature* **467**, 479–483 (2010).
41. L. I. Toledo, M. Altmeyer, M. B. Rask, C. Lukas, D. H. Larsen, L. K. Povlsen, S. Bekker-Jensen, N. Mailand, J. Bartek, J. Lukas, ATR prohibits replication catastrophe by preventing global exhaustion of RPA. *Cell* **155**, 1088–1103 (2013).
42. M. Kai, M. N. Boddy, P. Russell, T. S.-F. Wang, Replication checkpoint kinase Cds1 regulates Mus81 to preserve genome integrity during replication stress. *Genes Dev.* **19**, 919–932 (2005).
43. M. Segurado, J. F. X. Diffley, Separate roles for the DNA damage checkpoint protein kinases in stabilizing DNA replication forks. *Genes Dev.* **22**, 1816–1827 (2008).
44. I. Miyabe, T. Morishita, H. Shinagawa, A. M. Carr, *Schizosaccharomyces pombe* $Cds1^{Chk2}$ regulates homologous recombination at stalled replication forks through the phosphorylation of recombination protein Rad60. *J. Cell Sci.* **122**, 3638–3643 (2009).
45. F. B. Couch, C. E. Bansbach, R. Driscoll, J. W. Luzwick, G. G. Glick, R. Bétous, C. M. Carroll, S. Y. Jung, J. Qin, K. A. Cimprich, D. Cortez, ATR phosphorylates SMARCAL1 to prevent replication fork collapse. *Genes Dev.* **27**, 1610–1623 (2013).
46. E. J. Brown, D. Baltimore, ATR disruption leads to chromosomal fragmentation and early embryonic lethality. *Genes Dev.* **14**, 397–402 (2000).
47. A. de Klein, M. Muijtjens, R. van Os, Y. Verhoeven, B. Smit, A. M. Carr, A. R. Lehmann, J. H. Hoeijmakers, Targeted disruption of the cell-cycle checkpoint gene ATR leads to early embryonic lethality in mice. *Curr. Biol.* **10**, 479–482 (2000).
48. Q. Liu, S. Guntuku, X. S. Cui, S. Matsuoka, D. Cortez, K. Tamai, G. Luo, S. Carattini-Rivera, F. DeMayo, A. Bradley, L. A. Donehower, S. J. Elledge, Chk1 is an essential kinase that is regulated by Atr and required for the G_2/M DNA damage checkpoint. *Genes Dev.* **14**, 1448–1459 (2000).
49. K. A. Cimprich, D. Cortez, ATR: An essential regulator of genome integrity. *Nat. Rev. Mol. Cell Biol.* **9**, 616–627 (2008).
50. L. M. Phan, A.-H. Rezaeian, ATM: Main features, signaling pathways, and its diverse roles in DNA damage response, tumor suppression, and cancer development. *Genes (Basel)* **12**, 845 (2021).
51. W. W. Hwang, S. Venkatasubrahmanyam, A. G. Ianculescu, A. Tong, C. Boone, H. D. Madhani, A conserved RING finger protein required for histone H2B monoubiquitination and cell size control. *Mol. Cell* **11**, 261–266 (2003).
52. P. S. Freemont, RING for destruction? *Curr. Biol.* **10**, R84–R87 (2000).
53. B. Zhu, Y. Zheng, A.-D. Pham, S. S. Mandal, H. Erdjument-Bromage, P. Tempst, D. Reinberg, Monoubiquitination of human histone H2B: The factors involved and their roles in HOX gene regulation. *Mol. Cell* **20**, 601–611 (2005).
54. Z.-H. Deng, H.-S. Ai, C.-P. Lu, J.-B. Li, The Bre1/Rad6 machinery: Writing the central histone ubiquitin mark on H2B and beyond. *Chromosome Res.* **28**, 247–258 (2020).
55. M. Zofall, S. I. S. Grewal, HULC, a histone H2B ubiquitinating complex, modulates heterochromatin independent of histone methylation in fission yeast. *J. Biol. Chem.* **282**, 14065–14072 (2007).
56. L. Oss-Ronen, T. Sarusi, I. Cohen, Histone mono-ubiquitination in transcriptional regulation and its mark on life: Emerging roles in tissue development and disease. *Cells* **11**, 2404 (2022).
57. C. C. So, S. Ramachandran, A. Martin, E3 ubiquitin ligases RNF20 and RNF40 are required for Double-Stranded Break (DSB) repair: Evidence for monoubiquitination of histone H2B lysine 120 as a novel axis of DSB signaling and repair. *Mol. Cell. Biol.* **39**, e00488-18 (2019).
58. K. G. Kolobynina, A. Rapp, M. C. Cardoso, Chromatin ubiquitination guides DNA double strand break signaling and repair. *Front. Cell Dev. Biol.* **10**, 928113 (2022).
59. G. Goldstein, M. Scheid, U. Hammerling, D. H. Schlesinger, H. D. Niall, E. A. Boyse, Isolation of a polypeptide that has lymphocyte-differentiating properties and is

probably represented universally in living cells. *Proc. Natl. Acad. Sci. U.S.A.* **72**, 11–15 (1975).
60. I. Kouranti, J. R. McLean, A. Feoktistova, P. Liang, A. E. Johnson, R. H. Roberts-Galbraith, K. L. Gould, A global census of fission yeast deubiquitinating enzyme localization and interaction networks reveals distinct compartmentalization profiles and overlapping functions in endocytosis and polarity. *PLOS Biol.* **8**, e1000471 (2010).
61. Z. C. Elmore, J. R. Beckley, J. S. Chen, K. L. Gould, Histone H2B ubiquitination promotes the function of the anaphase-promoting complex/cyclosome in *Schizosaccharomyces pombe*. *G3 (Bethesda)* **4**, 1529–1538 (2014).
62. G.-J. Seo, S.-E. Kim, Y.-M. Lee, J.-W. Lee, J.-R. Lee, M.-J. Hahn, S.-T. Kim, Determination of substrate specificity and putative substrates of Chk2 kinase. *Biochem. Biophys. Res. Commun.* **304**, 339–343 (2003).
63. A. Lopez-Girona, K. Tanaka, X. B. Chen, B. A. Baber, C. H. McGowan, P. Russell, Serine-345 is required for Rad3-dependent phosphorylation and function of checkpoint kinase Chk1 in fission yeast. *Proc. Natl. Acad. Sci. U.S.A.* **98**, 11289–11294 (2001).
64. T. O'Neill, L. Giarratani, P. Chen, L. Iyer, C.-H. Lee, M. Bobiak, F. Kanai, B.-B. Zhou, J. H. Chung, G. A. Rathbun, Determination of substrate motifs for human Chk1 and hCds1/Chk2 by the oriented peptide library approach. *J. Biol. Chem.* **277**, 16102–16115 (2002).
65. A. Zukowski, A. M. Johnson, The interplay of histone H2B ubiquitination with budding and fission yeast heterochromatin. *Curr. Genet.* **64**, 799–806 (2018).
66. L. T. Bailey, S. J. Northall, T. Schalch, Breakers and amplifiers in chromatin circuitry: Acetylation and ubiquitination control the heterochromatin machinery. *Curr. Opin. Struct. Biol.* **71**, 156–163 (2021).
67. S. Machida, S. Sekine, Y. Nishiyama, N. Horikoshi, H. Kurumizaka, Structural and biochemical analyses of monoubiquitinated human histones H2B and H4. *Open Biol.* **6**, 160090 (2016).
68. F. Thoma, Mapping of nucleosome positions. *Methods Enzymol.* **274**, 197–214 (1996).
69. J. Cao, Q. Yan, Histone ubiquitination and deubiquitination in transcription, DNA damage response, and cancer. *Front. Oncol.* **2**, 26 (2012).
70. R. Pavri, B. Zhu, G. Li, P. Trojer, S. Mandal, A. Shilatifard, D. Reinberg, Histone H2B monoubiquitination functions cooperatively with FACT to regulate elongation by RNA polymerase II. *Cell* **125**, 703–717 (2006).
71. A. Zukowski, N. O. Al-Afaleq, E. D. Duncan, T. Yao, A. M. Johnson, Recruitment and allosteric stimulation of a histone-deubiquitinating enzyme during heterochromatin assembly. *J. Biol. Chem.* **293**, 2498–2509 (2018).
72. M. Nune, M. T. Morgan, Z. Connell, L. McCullough, M. Jbara, H. Sun, A. Brik, T. Formosa, C. Wolberger, FACT and Ubp10 collaborate to modulate H2B deubiquitination and nucleosome dynamics. *eLife* **8**, e40988 (2019).
73. H. T. Korenfeld, A. Avram-Shperling, Y. Zukerman, A. Iluz, H. Boocholez, L. Ben-Shimon, S. Ben-Aroya, Reversal of histone H2B mono-ubiquitination is required for replication stress recovery. *DNA Repair (Amst)* **119**, 103387 (2022).
74. G. Fuchs, D. Hollander, Y. Voichek, G. Ast, M. Oren, Cotranscriptional histone H2B monoubiquitylation is tightly coupled with RNA polymerase II elongation rate. *Genome Res.* **24**, 1572–1583 (2014).
75. M. K.-W. Ma, C. Heath, A. Hair, A. G. West, Histone crosstalk directed by H2B ubiquitination is required for chromatin boundary integrity. *PLOS Genet.* **7**, e1002175 (2011).
76. M. B. Chandrasekharan, F. Huang, Z.-W. Sun, Ubiquitination of histone H2B regulates chromatin dynamics by enhancing nucleosome stability. *Proc. Natl. Acad. Sci. U.S.A.* **106**, 16686–16691 (2009).
77. V. Gaggioli, C. S. Y. Lo, N. Reverón-Gómez, Z. Jasencakova, H. Domenech, H. Nguyen, S. Sidoli, A. Tvardovskiy, S. Uruci, J. A. Slotman, Y. Chai, J. G. S. C. Souto Gonçalves, E. M. Manolika, O. N. Jensen, D. Wheeler, S. Sridharan, S. Chakrabarty, J. Demmers, R. Kanaar, A. Groth, N. Taneja, Dynamic de novo heterochromatin assembly and disassembly at replication forks ensures fork stability. *Nat. Cell Biol.* **25**, 1017–1032 (2023).
78. S. Scherer, R. W. Davis, Replacement of chromosome segments with altered DNA sequences constructed in vitro. *Proc. Natl. Acad. Sci. U.S.A.* **76**, 4951–4955 (1979).
79. M. Muzi Falconi, A. Piseri, M. Ferrari, G. Lucchini, P. Plevani, M. Foiani, De novo synthesis of budding yeast DNA polymerase α and POL1 transcription at the G1/S boundary are not required for entrance into S phase. *Proc. Natl. Acad. Sci. U.S.A.* **90**, 10519–10523 (1993).
80. C. Janke, M. M. Magiera, N. Rathfelder, C. Taxis, S. Reber, H. Maekawa, A. Moreno-Borchart, G. Doenges, E. Schwob, E. Schiebel, M. Knop, A versatile toolbox for PCR-based tagging of yeast genes: New fluorescent proteins, more markers and promoter substitution cassettes. *Yeast* **21**, 947–962 (2004).
81. B.-S. Lee, J.-S. Huang, G. D. L. P. Jayathilaka, S. S. Lateef, S. Gupta, Production of antipeptide antibodies. *Methods Mol. Biol.* **657**, 93–108 (2010).
82. A. J. Archuleta, C. A. Stutzke, K. M. Nixon, M. D. Browning, Optimized protocol to make phospho-specific antibodies that work. *Methods Mol. Biol.* **717**, 69–88 (2011).
83. R. P. Duren, S. P. Boudreaux, O. M. Conneely, Genome wide mapping of NR4A binding reveals cooperativity with ETS factors to promote epigenetic activation of distal enhancers in acute myeloid leukemia cells. *PLOS ONE* **11**, e0150450 (2016).
84. J. N. Bianco, J. Poli, J. Saksouk, J. Bacal, M. J. Silva, K. Yoshida, Y.-L. Lin, H. Tourrière, A. Lengronne, P. Pasero, Analysis of DNA replication profiles in budding yeast and mammalian cells using DNA combing. *Methods* **57**, 149–157 (2012).

Acknowledgments: We thank all members of the Kong Laboratory for discussions and support, Z. Li and J. Ji for help with MS analysis, and L. Bruce for English editing. We thank the National Center for Protein Sciences (Beijing) at Peking University for assistance with flow cytometry and fluorescent imaging. We thank L. Du for providing *S. pombe* strains LD330 (*wt*), LD297 (*rad3*Δ), *ubp8*Δ, and DY683. We thank A. Carr for providing *S. pombe* strains Ets13 (*cds1*Δ) and J2172. We also thank C. Liu for providing *S. pombe* strains *htb1*-3FLAG and *htb1-K119R*-3FLAG. **Funding:** This work was supported by grants from the Ministry of Science and Technology of China (2016YFA0500301) and the National Natural Science Foundation of China (nos. 31230021 and 32250710143) awarded to D.K. This work was also supported by the Peking-Tsinghua Center for Life Sciences and the National Key Laboratory of Protein and Plant Gene Research. **Author contributions:** Conceptualization: D.K., X. Li, and C.L.; methodology and investigation: X. Liu performed most assays, including a large portion of experimental designs and writing; B.Z. also made substantial contributions to this study, including experiments, writing, review, and editing; Y.H. performed genetic screening and obtained the *brl2-Q236** mutation; D.K., X. Li, and C.L. supervised the study and writing. Funding acquisition: D.K. **Competing interests:** The authors declare that they have no competing interests. **Data and materials availability:** All data needed to evaluate the conclusions in the paper are present in the paper and/or the Supplementary Materials.

Submitted 27 June 2024
Accepted 17 April 2025
Published 16 May 2025
10.1126/sciadv.adr3673